Master Thesis

A method to obtain macroscopic plastic strain values with Electron Backscatter Diffraction data and a comparison with FEM

Remy Ripandelli
s2249855

Supervisors:

Dr. ir. I. Basu
Dr. ir. V. Ocelík
Prof. Dr. J. Th. M. De Hosson

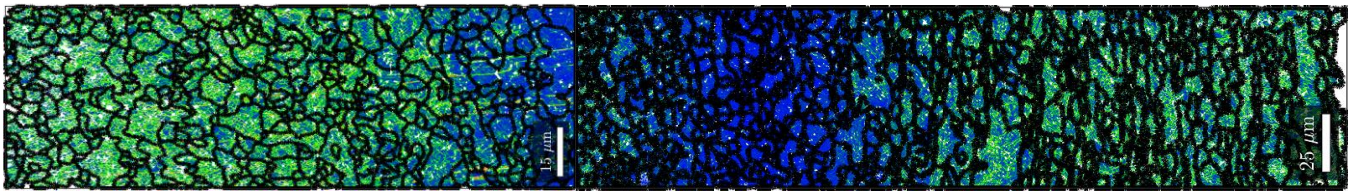

2018

Rijksuniversiteit Groningen

Abstract

In this study EBSD scanned misorientations of a highly deformed ferritic metal was used to calculate quantitative macroscopic plastic strain values using a statistical approach. By using EBSD measurements on tensile test samples, a correlation between the misorientation values and macroscopic plastic strain was found. Misorientation values measured on various highly deformed bent samples were translated in macroscopic plastic strain values using the correlation equation. The bent samples were simulated with a finite element model and the experimental values agreed very well with the computed data. Furthermore an attempt was made to calculate the microscopic misorientation data with a very simplified dislocation density model which treats all misorientation values as measures for glide dislocations. The resulting microscopic strain values obtained were in the order of 10^1. This approach was too straight forward because misorientations result from a very complex interaction of different kind of dislocations. It was therefore rejected. Finally a study of the reliability of the used equipment was done in the form of a gage repeat and reproducibility study which revealed a total relative error of misorientations that did not exceed 0.8 %.

Contents

1 Introduction

In the last three decades the use material characterization techniques has evolved to study elastic and plastic deformations in metals. The principle is the measurements of lattice deformations in the crystal. Transmission electron microscopy (TEM) provides the highest resolution so far and is ideal for intra grain, or very local, dislocation studies. However it is not suitable for statistical studies. Neutron diffraction and electron backscatter diffraction (EBSD) are techniques able to gather data faster, but with less resolution. The former can be used to study bulk sample in three dimensions and requires a synchrotron accelerator. The latter is a more available technique suitable for surface characterization. This technique is used to study the diffraction pattern quality or to study the misorientations of the crystal lattices. These misorientations are a measure for lattice deformations. It has been proven that tensile tests correlate with misorientations to macroscopic plastic strains. [1] Studies to investigate the relation between misorientations and microscopic plastic strain include techniques to estimate dislocation densities and influences of averaging techniques and EBSD step size settings. [2-8]

At Philips a material model was developed for a ferritic AISI 420 like steel. This model is used with finite element modelling for the designs of shaving caps and consists of in-house physical and mechanical measurements. [11] Validations of computed plastic strains have yet to be done. This requires a method of interpreting experimentally measured microscopic variables and translating them into macroscopic values. Real metals have a grain structure with many complex behaviors of dislocations. This is in contrast to a finite element model which omits these microscopic complexities and uses block shaped elements to compute macroscopic values using the classical constitutive equations.

A translation of misorientation data into macroscopic plastic strain values is therefore needed. The many complex effects dislocations can encounter during a deformation makes an accurate calculation of microscopic plastic strain, and especially macroscopic plastic strain, a challenging task. Therefore a statistical empirical approach is needed. Large quantities of misorientation data could reveal the results of the dominant deformation behavior.

In this study a translation needs to be made from misorientations to microscopic plastic strain with the use of a correlation model obtained with tensile tests. The quality of this approach has to be tested in various more complex deformed samples rather than tensile test samples. These samples have to be heavily deformed in such a way that the plastic strains are still relatively easy to interpret. The large data sets obtained from these more complex samples then have to be compared with the computed finite element modelling data. An attempt will be made to calculate the microscopic plastic strain using the misorientation data by treating the latter as a direct result of glide dislocations only. This is a very crude model that ignores the highly complex interactions of different kind of dislocations that give rise to the misorientations and serves to investigate whether it will give a least a correct indication of microscopic plastic strain values. Finally a gage repeat and reproducibility study has to be done to investigate the reliability of the EBSD scans.

2 Theory

In this chapter the basic theory of dislocations and slip systems in plastic deformations is explained. It is followed by the Orowan's equation which is central in this study. After this theory the concept of electron backscatter diffraction measurements and the definition of misorientations is explained. Finaly a simplified model to translate misorientations in dislocation densities is discussed based on [2-4].

2.1 Dislocations

Defects in the crystal lattice of a metal cause ductility. Figure 1 illustrates the principle of a defect. Above and under the defect the local lattice is compression strained and tensile strained respectively. This causes stress fields around the defect. When a shear stress is applied the bond around the defect rearrange causing the defect to travel from one side to the other. When the defect reaches the side the lattice above it will have shifted a length known as the Burger's vector. The lattice is now plastically deformed.

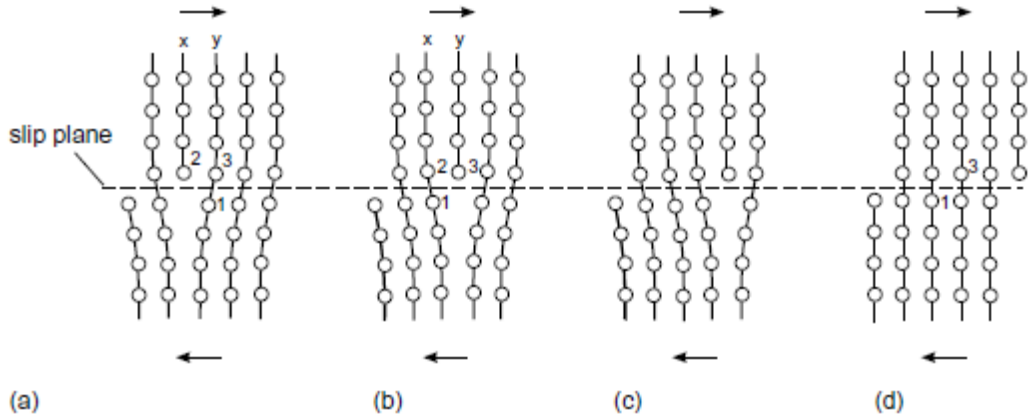

Figure 1 An illustration of the edge dislocation movement. [9] The arrow indicates the applied shear stress. The movement starts in a) and ends in d).

When the defect in Figure 1 forms a line into the page it is called a line defect, or dislocation. This is a one dimensional defect whereas a zero dimensional defect is a lattice vacancy. The sign of the dislocation is determined by the direction in which they travel in the lattice plane. Edge dislocations have a line defect perpendicular to the Burgers vector while screw dislocations have a line defect parallel to the Burgers vector. Figure 2 shows the difference between the two. This conservative motion of dislocations is called glide and occurs with no change in volume. Alternatively climb is non conservative and a volume change is introduced. In the latter case a dislocation changes lattice planes during movement. The theory of these defects was originally developed by the Italian mathematician and physicist Vito Volterra in 1907 and the term dislocations was coined by the British mathematician and physicist Sir Geoffrey Ingram Taylor in 1934.

Plastic deformation of crystalline solids is most commonly manifested by glide. A high number of dislocations gliding in a slip plane is called slip. This slip plane is the plane orientation that is most densely packed of the crystal configuration. The spacing between these plane orientations is the largest of all orientations causing movement between the planes to occur with the least resistance. For the same

reason the direction in which the dislocations move is the direction of the smallest displacement distance of atoms in the plane.

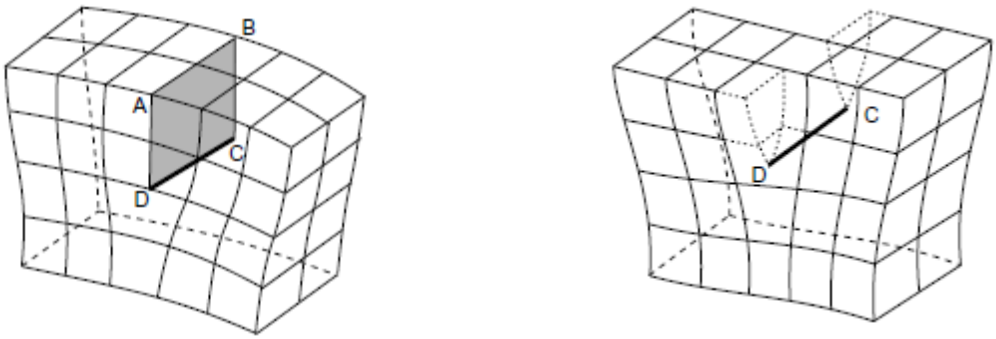

a b

Figure 2 the differences between a) an edge dislocation and b) a screw dislocation.

There are different slip planes in a crystal configuration and when a stress is applied the plane with the orientation that requires the least stress to overcome the resistance will be active first. Figure 3 shows an illustration of a tensile test and the active slip plane. The resultant stress applied on the dislocations in the slip plane is derived with equation 1.

$$\tau = \frac{F}{A}\cos\phi\cos\lambda \tag{1}$$

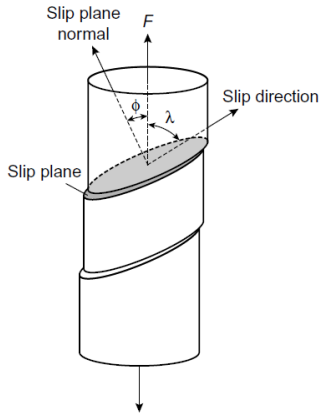

Figure 3 A schematic illustration of the slip planes and directions during a tensile test.

where τ is the residual stress, F is the applied force, A is the cross section area, ϕ is the angle between F and the slip plane normal and λ is the angle between F and the slip plane direction.

Here the product of the cosine terms is called the Schmid factor. A metal sample consists of lattice domains, called grains, with different orientations. These grains are separated by grain boundaries where the lattice orientations typically differ more than 10 degrees. So when a stress is applied the principle illustrated in Figure 3 can occur in each grain differently depending on the orientation of the lattice.

A body centered cubic crystal, depicted in Figure 4, has six primary slip planes {110} and four slip directions <111> in each plane giving 24 combinations called slip systems.

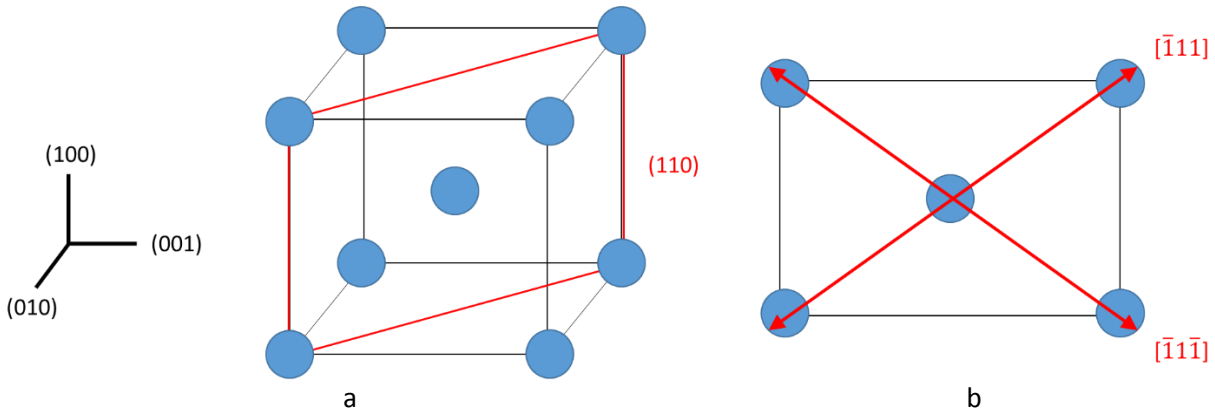

Figure 4 The body centered cubic (BCC) with a) one of the six primary slip planes {110} highlighted and b) two of the slip directions <111>.

When bending a metal sample the randomly distributed dislocations in a grain will start to rearrange. They move on their slip planes to eventually form a new edge. This is illustrated in Figure 5. At this edge the two separated parts, called cells, differ not more than two degrees in orientation. This type of edge is called a low angle boundary. This is the first step of the formation of low angle sub grains.

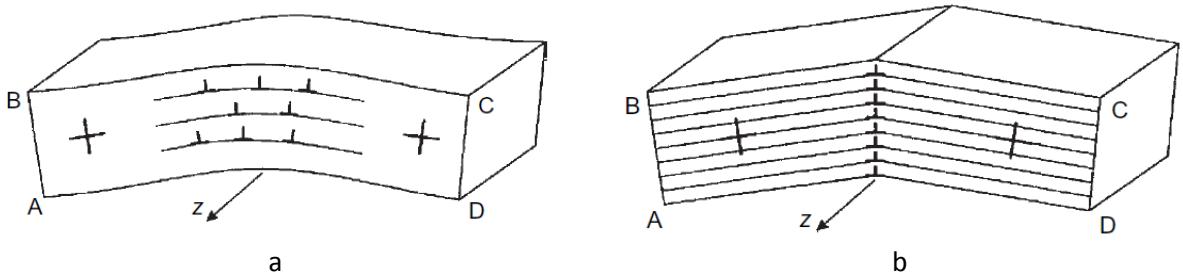

Figure 5 The formation of a low angle boundary. The slip directions are indicated by the crosses. a) At first the dislocations (indicated with a flipped 'T') are distributed randomly. b) The sample is bent and the dislocations rearrange to form a symmetrical tilt boundary. [9]

During plastic deformation a shear stress is applied to the slip plane and dislocations will glide via the slip planes towards the grain boundaries. Here they will pile up due to the high stresses caused by the orientation difference with the adjacent grain. The dislocations could cross the boundary but that would require a lot more energy. As explained earlier each dislocation has a stress field around it. Due to the piled up the accumulation and higher concentration of dislocations cause a large stress field as well. Because of the applied shear stress on the bulk sample dislocations move and can nucleate new dislocations as well. This is caused by dislocations, or defect lines, being pinned at certain points while the rest of the line continues moving. The lines can be pinned down by parts of the line that climbed to another slip plane that are non-active at the moment, or by impurities in the crystal. This is known as Frank Read sources after the British physicists Charles Frank and Thornton Read who published it in 1950. Other ways dislocations nucleate happen at the boundaries due to the imperfections introduced by the plastic deformation of the grain and the interaction with neighboring grains. These dislocations can cross to the next grain, be trapped in the boundary and will introduce more strain, or they travel into the current grain.

As a whole existing and newly nucleated dislocations move and the dislocation density increases. Due to the repulsive forces of higher (local) dislocation densities it becomes more and more difficult to move dislocations towards the boundaries. Therefore more energy is required making the metal as a bulk stronger and harder to permanently deform. In this process low angle boundaries could be formed dividing the grain in separate cells. There boundaries will contribute to the increase in the required energy as well. After deformation there will be a distribution of dislocations in the grain with dislocation densities increasing towards the grain boundaries. The strength has increased and the ductility has decreased. This process of plastic deformation at room temperatures is called cold work and the effect it has on the metal is called strain, or work hardening.

There is a distinction between geometrically necessary dislocations (GND) which are dislocations of the same sign that accumulate to accommodate for the lattice curvature in deformations, and statistically stored dislocations (SSD) which are dislocations of either sign that can accumulate or can annihilate each other. The former is not the type of dislocations seen in glide. The distinction between the two types is very hard to make when examining misorientations. This is why an empirical relation between misorientations and macroscopic plastic strain is used in this study.

2.2 Orowan's Equation

Plastic deformation depends on the crystal structure of the material, temperature, strain rate, strain and the type of defects in the (poly) crystal and is therefore a complicated process. Orowan's equation is a simplified model that describes plastic strain caused by slip that is valid for glide and climb. It was developed by the Hungarian physicist Egon Orowan in 1934.

Figure 6 shows a crystal containing edge dislocations on which a stress is applied. When the shear stress exceeds the critical resolved shear stress of the primary slip plane, the plane will become active and the already existing dislocations will start to move. A dislocation that travels distance x on the plane will have contributed the fraction of x/d of one burgers vector of deformation with d the length of the plane. Many (N) dislocation will contribute in this manner and the result is a macroscopic displacement here denoted as D.

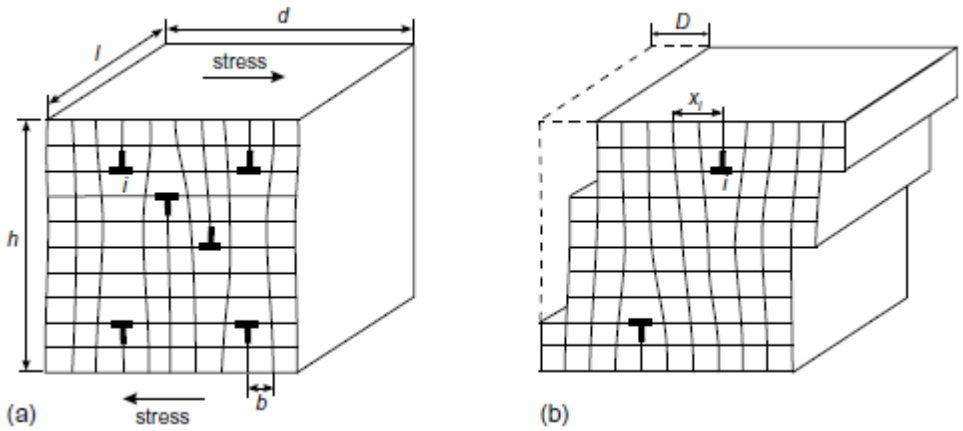

Figure 6 An illustration of the concept of edge dislocation movement causing plastic deformation where a) represents the initial state with the applied shear stresses indicated by the arrows and b) the final deformed state. [9]

This deformation can be expressed as

$$D = \frac{b}{d}\sum_{i=1}^{N} x_i \tag{2}$$

This can be simplified further by taking the average distance a dislocation travels:

$$\bar{x} = \frac{1}{N}\sum_{i=1}^{N} x_i \tag{3}$$

By definition the macroscopic plastic shear strain is defined as

$$\gamma_p = \frac{D}{h} \tag{4}$$

Based on Figure 6b an expression for the dislocation density is

$$\rho_{dislocation} = \frac{Nl}{hld} \tag{5}$$

Combining everything gives a relation involving an expression for the dislocation density. The Orowan expression for plastic strain therefore is

$$\varepsilon_p = b\,\rho_{dislocation}\,\bar{x} \tag{6}$$

This simplified model relates plastic strain with an average distance travelled and with an estimate of the dislocation density. The principle illustrated in Figure 6 is also applicable to screw and climb dislocations. It does not contain any information about dislocation nucleation or dislocation type (edge and screw) or dislocation movement (glide and climb). It simply describes the resulting plastic strain caused by dislocation movement over an average distance regardless whether they already existed or where nucleated.

2.3 Electron Backscatter Diffraction

Electron backscatter diffraction, or EBSD, is a technique in which backscatter electrons are used to project diffraction patterns of a crystal surface on a detector. Using a scanning electron microscope (SEM) electrons are accelerated with energies in the range of 5 to 30 keV on a sample. Backscattered electrons are electrons deflected elastically by the nuclei of the sample. Since the incoming electrons can experience many scattering events, the sample is tilted about 70 ° with respect to the electron beam thereby reducing the absorption and enhancing the resulting backscattered electron signal. They create a diffraction pattern on the detector called Kikuchi patterns. Figure 7 shows the steps from a Kikuchi pattern (Figure

7a) to a Hough peak and is used in the following short description of how the crystal orientation is determined using the diffraction pattern. [10]

The center line of the detected bands in Figure 7c can be described by the coordinates of that line using

$$y = \frac{\rho}{\sin\varphi} + \frac{\cos\varphi}{\sin\varphi}x \tag{7}$$

which can be rewritten as

$$\rho = x\cos\varphi + y\sin\varphi \tag{8}$$

A straight line has a constant combination of ρ and φ. (See Figure 7b to 7d) The bands detected form a set of combinations forming the Hough transform of the diffraction pattern. Figures 7e and 7f show the calculation of a Hough peak and an example of the Hough transform respectively.

Next the screen coordinates of the pattern are translated to specimen coordinates and the third dimension is added using the specimen to screen distance illustrated in Figure 8. Equation 9 is the relation used in which matrix A incorporates the differences between the microscope, detector and specimen axes.

$$\boldsymbol{r} = x_s y_s z_s = \boldsymbol{A}\,(x - x_{PC}, y - y_{PC}, SSD) \tag{9}$$

The lattice planes and the orientation of the lattice with which the detected Kikuchi bands correspond have to be identified. The angle of the Kikuchi bands are now known in specimen coordinates and the angles between intersecting bands are calculated and compared with a lookup table of all known interplanar angles between the low Miller indices planes of the crystal structure, including every plane of the family of planes. The match also reveals the crystal coordinates of the lattice. This is known as pattern indexing.

Now that the crystal coordinates and the specimen coordinates are known, the 3x3 **g** matrix is obtained which contains the crystallographic orientation of the crystal. This is done using three pairs (crystal and specimen axes) of vector r. (See equation 9) The following equation is solved:

$$\boldsymbol{r}_c = \boldsymbol{g} \bullet \boldsymbol{r}_s \tag{10}$$

The orientation is defined by matrix **g** which is the transformation between the crystal and specimen system via angles called Euler angles. The Euler angles are a set of three angles describing the orientation of the crystal reconstructed from the Kikuchi pattern. This is the output of an EBSD scan.

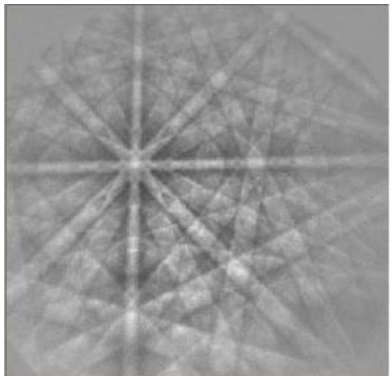

a

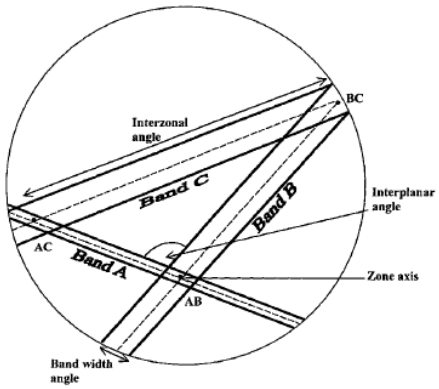

b

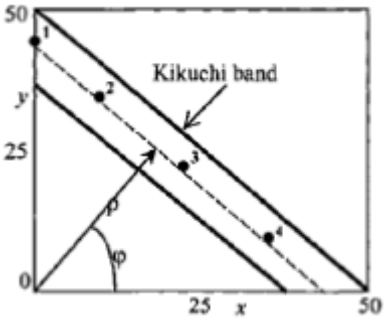

c

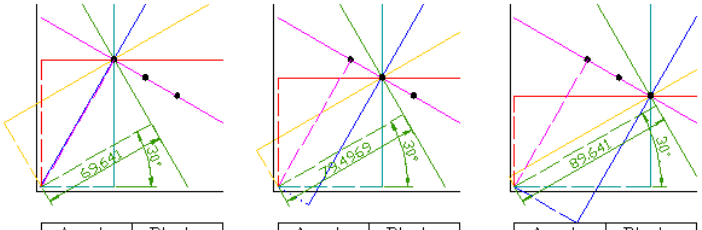

Angle	Dist.
0	40
30	69.6
60	81.2
90	70
120	40.6
150	0.4

Angle	Dist.
0	57.1
30	79.5
60	80.5
90	60
120	23.4
150	-19.5

Angle	Dist.
0	74.6
30	89.6
60	80.6
90	50
120	6.0
150	-39.6

d

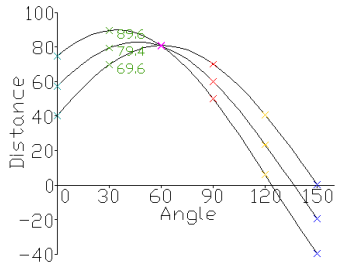

e

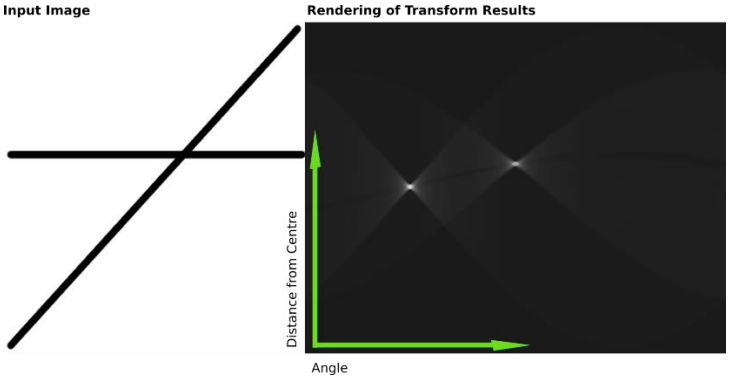

f

Figure 7 The pattern recognition principle of EBSD. a) A Kikuchi pattern. b) The Kikuchi bands detected by image recognition. c & d) The determination of the band angle. e) The determination of a Hough peak. f) The resulting Hough pattern of two bands illustrated left of the pattern.

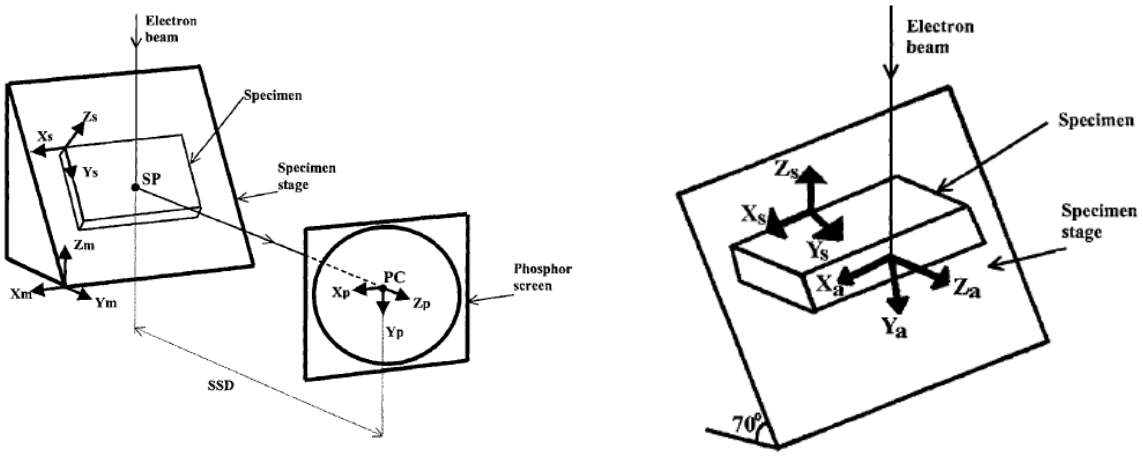

Figure 8 a) A schematic of the microscope stage, the sample and the detector. b) The specimen stage is tilted to about 70 °.

2.4 Misorientations

In the previous section the measurement of the crystal orientation was discussed. The output of an EBSD measurement of one pixel is a set of three Euler angles that describe the orientation in three dimensional space. In order to interpret the data one has to use a reference direction expressed in Miller indices. The crystallographic orientation of the crystal is than given with respect to the used reference direction. This could be for example [0 0 1]. When comparing the orientations of two pixels a common direction of the two is searched. It is with respect to this common direction (that does not have to be [0 0 1] in this example) that the difference in orientation (calculated with the Euler angles) between the two pixels is calculated. This difference is called misorientation. When requesting the misorientation between two pixels the output is two sets of Euler angles that can differ, the common direction and the calculated misorientation.

The misorientation of neighboring pixels is used for multiple purposes. The first is to detect when this misorientation exceeds a certain threshold that is set to distinguish grains. Neighbor pixel misorientations that differ more than a set threshold angle are recognized as grain boundaries. The second purpose is to study the misorientations below the threshold value. This information describes small deformations within a grain. It is the latter that is used in this study to be correlated with macroscopic plastic strain. To do so a model is needed to translate the misorientation data into dislocation densities. A model will be described in the next section.

Figure 9 shows an inverse pole Figure of an EBSD scan. The legend shows how the colors describe the orientations with respect to the [0 0 1] direction. A line (indicated in red) of misorientation data is requested that crosses two grain boundaries. For clarification a few cubes are shown in Figure 9 as well. These are visualizations that represent the crystal orientations of a pixel. It is clear how these orientations differ at different points. The second and the third cube show a small difference in orientation within the same grain.

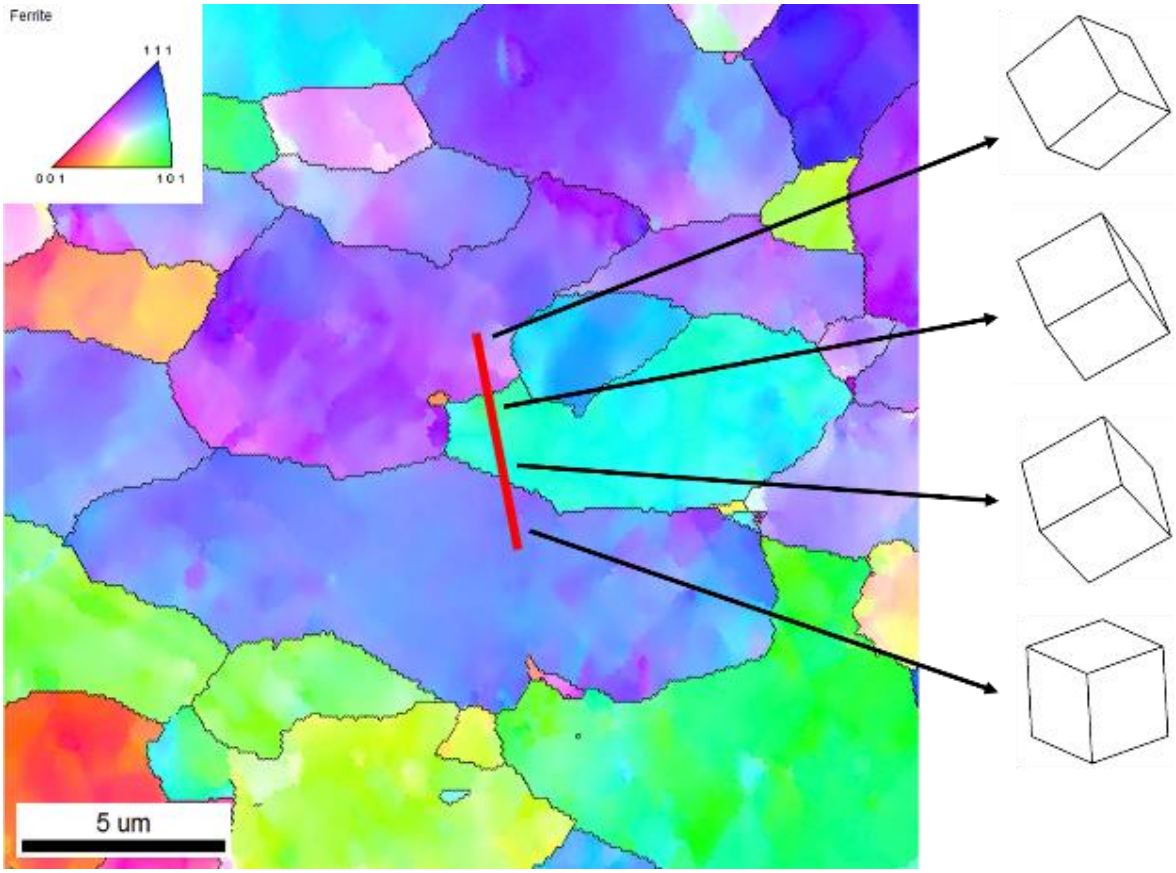

Figure 9 An inverse pole figure showing the crystallographic orientations of a ferritic sample with respect to the [0 0 1] direction. The red line indicates the pixels used to plot the misorientations shown in Figure 10. On the right side examples are given orientations of four pixels.

Figure 10 shows the data presented as the misorientation of each pixel along the line with respect to the first pixel (point to origin), and as the misorientation of each pixel with respect to its direct previous neighbor (point to point). The point to origin data shows clear steps in misorientations as we move further away from the first pixel. This is because when crossing a grain boundary the misorientation exceeds the grain boundary threshold value. The pixels in the next grain in general have a very different orientation compared to the neighboring grain. The point to point data shows how some pixels differ more in orientation than others. At the grain boundaries large peaks are observed as by definition the misorientations should exceed the set threshold.

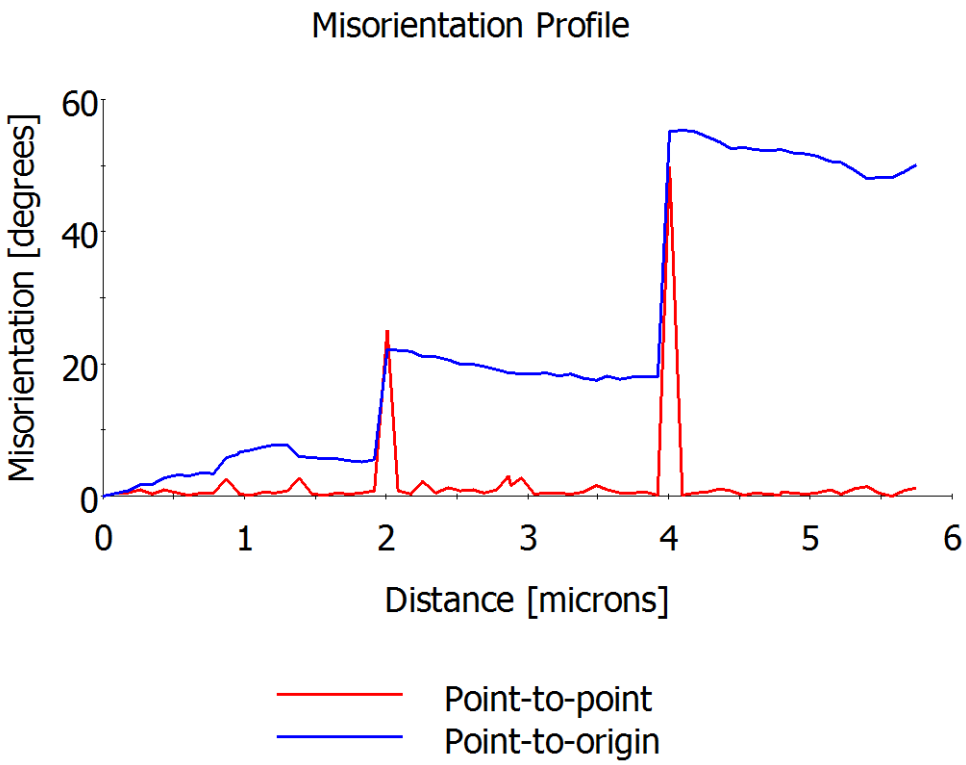

Figure 10 The misorientations of the pixel along the red line in Figure 9.

The kernel average misorientation (KAM) is the average value of the misorientations of a pixel with all its neighbors. This can be done for its direct neighbors or for a larger kernel including further neighbors. In this study we use the KAM level 1 which takes the average of the direct neighbors only. Figure 11 shows a zoomed in example of the KAM 1 map of Figure 9. The hexagonal pixel has six neighbors which are used to calculate the average misorientation. The value of the misorientation is indicated with a color. The two cubes show the orientations of the pixel and one of its neighbors. The KAM 1 is the misorientation data needed to estimate the dislocation density as will be explained in the next section.

In this study another type of processing is used to express misorientation data which is the mean misorientation with respect to the grain orientation. In this study this type of process is called MORI.

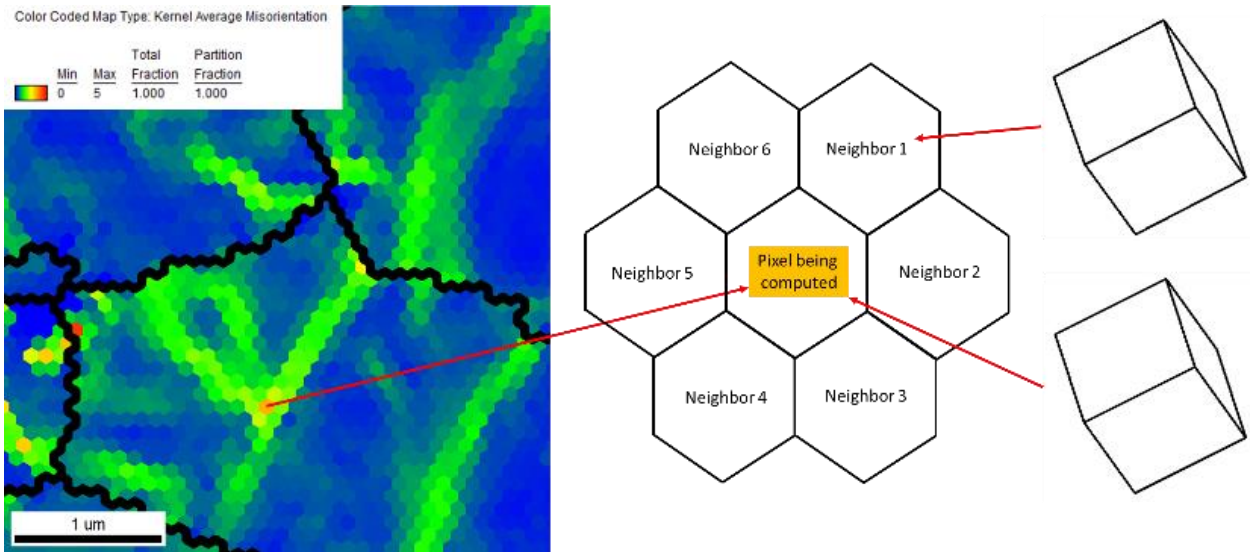

Figure 11 The zoomed in KAM 1 map of Figure 9. The colors are a measure for the average misorientation of the pixel with respect to its six neighbors. The cubes indicate a slight difference in orientation of one of its neighbors.

2.5 A Simplified Dislocation Density Model using EBSD

As explained in the introduction, next to the empirical relation between misorientations and macroscopic plastic strain, an attempt was made to calculate microscopic misorientations. The model for this attempt is explained in this section. The misorientations discussed in the previous section are widely used to study microscopic plastic deformation. (See the introduction) One model to estimate geometrically necessary dislocation densities is based on the number of dislocations estimated on the edges of EBSD scan pixels. [2-4] However, in this study the approach is used to model glide dislocation densities and is used with Orowan's equation. The crude assumption is made that the misorientations measured are a direct consequence of glide dislocations and ignores the fact that many different complex dislocation interactions are responsible for the lattice deformations.

In this approach each pixel of a scan is treated as a crystal as illustrated in Figure 6. The misorientations with the neighboring pixels is used to estimate the slip plane misorientations. Figure 12 shows a pixel from a kernel average misorientation (KAM) map. A square pixel is used here for simplicity. The edge length of the pixel is equal to the step size used during the scan.

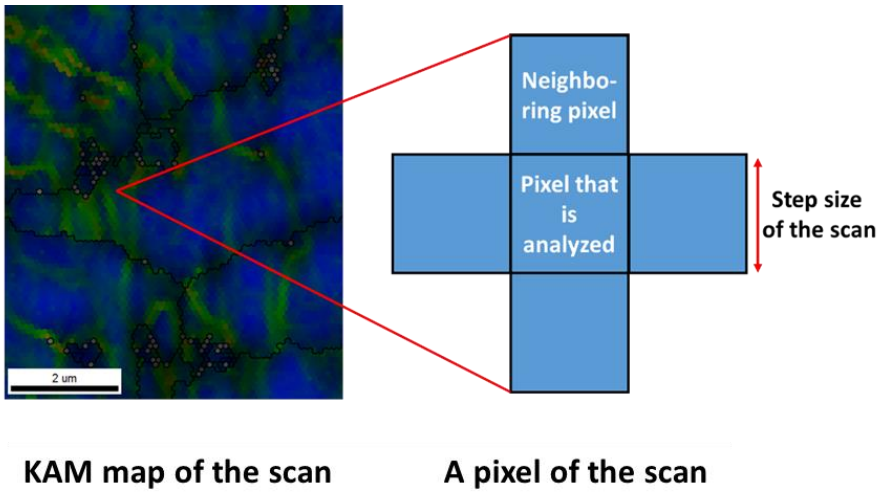

Figure 12 One pixel of a KAM map with its neighbor pixels.

The pixel in the middle is analyzed to calculate its dislocation density. When we zoom in at the boundary (See Figure 13) the steps of the slip planes can be seen. The assumption now is that they are all displaced by one Burgers vector. The misorientation between two pixels is considered to be the angle between their slip plane orientations. [2] [4]

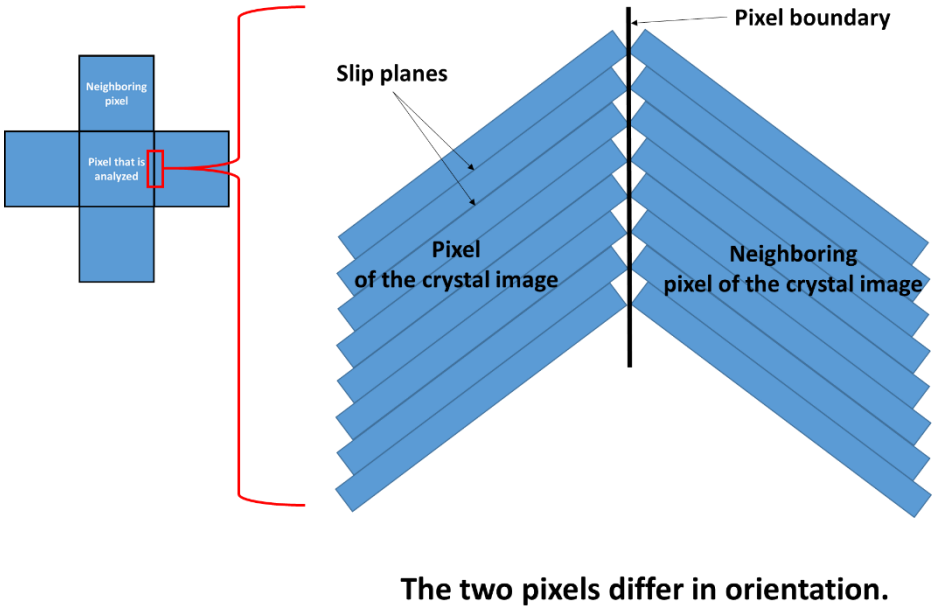

Figure 13 An illustration of the assumed slip planes at the border of the pixels.

Figure 14 zooms in further to show two slip planes at the boundary. Half of the misorientations angle and the burgers vector are used to calculate the part of the boundary facing the step.

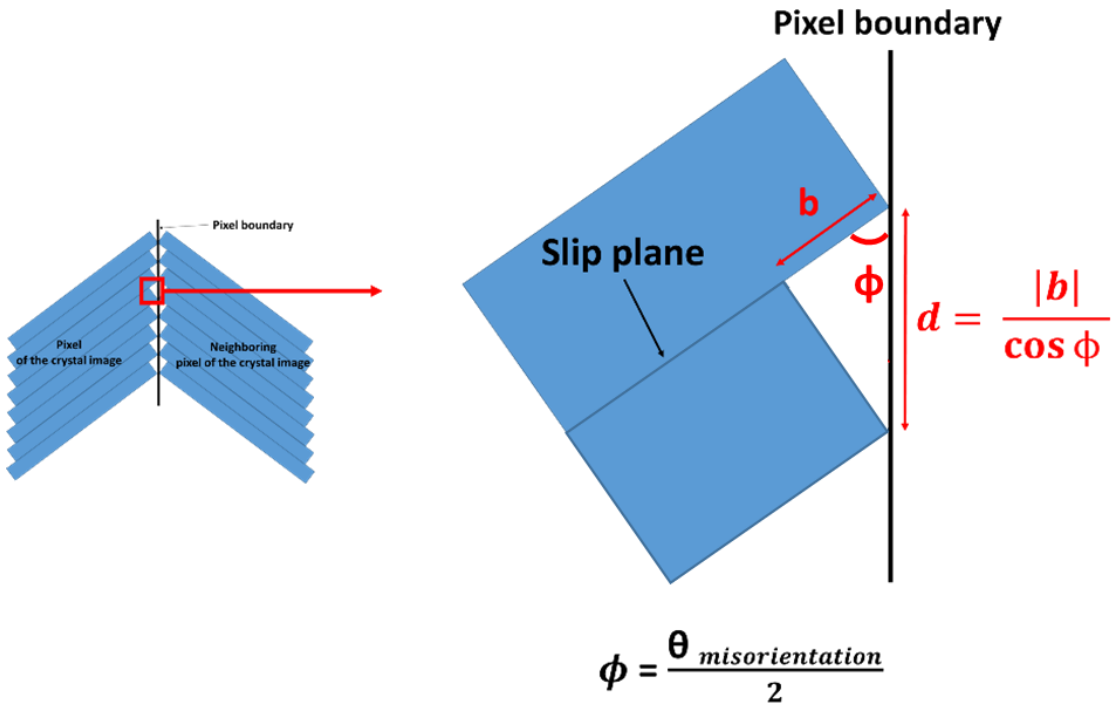

Figure 14 The calculation of the dislocation density along one pixel border. $\rho_{border} = \frac{a}{d}$ with *a* the step size.

This can be simplified for small angles by writing

$$d = \frac{|b|}{\cos\phi} \approx \frac{|b|}{\phi} \tag{11}$$

with b the Burgers vector of the of the slip plane and ϕ half of the misorientations angle at this boundary. Since each step is assumed to be created by one dislocation, the number of dislocations at this boundary is simply the boundary length divided by *d*. Repeating this for each of the four boundaries of this pixel and dividing by its area gives an estimate of the dislocation density of this pixel. The misorientation used for each boundary can be replaced by the mean misorientations of all the pixel's neighbors. This is the same as the kernel average misorientations (KAM) using kernel size one, which uses only the first neighbors. The derivation of one boundary can then simply be multiplied by the number of boundaries, in this case four.

$$n_{dislocation} = a\frac{\phi}{|b|} = a\frac{\theta_{mis}}{2|b|} \tag{12}$$

$$\rho_{pixel} = 4\,a\frac{\theta_{mis}}{2|b|}\frac{1}{a^2} = \frac{2\theta_{mis}}{a|b|} \tag{13}$$

where a is the step size used in the scan, θ_{mis} is the misorientation between the pixel and its neighbors and b is the Burger's vector which is taken to be the distance between two neighboring atom centers in the slip direction of the slip plane. This is repeated for each pixel to obtain a dislocation density data set of the scan.

3 Experimental Approach

In this study the relation between local crystal misorientations and macroscopic plastic strain is investigated. By doing a series of tensile tests and making EBSD scans of these samples a correlation is studied between the macroscopic plastic strain and the estimated microscopic plastic strain. To test this approach in a more general case, the coefficient of this correlation is then used to estimate the plastic strain of bended samples. The deformation that took place in these samples is more complex than that of tensile test samples and finite element calculations are used to compare the estimated results with the computational results. For the attempt to calculate the microscopic plastic strain, the dislocation density is estimated using a simplified model using the misorientations between two pixels of an EBSD scan. These are then used in the model of Orowan to calculate the microscopic plastic strain. Table 1 shows the steps taken in this approach.

Table 1. An overview of the steps taken.

Step	Activity
1	Performing tensile tests with defined macroscopic plastic strains.
2	EBSD scans with a small step size to map the misorientations.
3	Linear regression to estimate the misorientation versus macro plastic strain relation.
4	Performing bend tests with the same material.
5	EBSD scans with a small step size to map the misorientations.
6	Applying the misorientation versus macro plastic strain relation.
7	Comparison of experimentally obtained macrostrains with FEM simulations.
8	Calculate the microscopic plastic strain with Orowan's equation to test a simplified model with the assumption that the misorientations are a direct result of glide dislocations only.

In the first paragraph of this chapter the material and the samples of this study are described. The second paragraph discusses the hardware and the settings used. In the third paragraph the calculations for the dislocation density are adapted to the used EBSD settings. Finally a gage repeat and reproducibility test is presented to test the reliability of the scans made with this equipment.

3.1 Material and Samples

3.1.1 The Material

The material used in this study is a cold rolled strip steel named Sandvik 6C27. It is a martensitic stainless chromium steel with a low carbon content that is similar to AISI 420. Table 2 shows a comparison between the used material and AISI 420. The samples were prepared in the ferritic phase and therefore the calculations for the plastic strain are performed for a body centered cubic (BCC). (See Figure 4) The mechanical properties are summarized in Table 3 and were obtained from earlier tests [11].

Table 2. The chemical composition of Sandvik 6C27 and AISI 420 in weight percentages. [12]

	C	Cr	Si	Mn	P	S	Mo	Fe
Sandvik 6C27	0.32	13.7	0.2	0.30	≤0.025	≤0.010	-	Bal.
AISI 420	Min 0.15	12-14	1	1	0.04	0.030	-	Bal.

Table 3 The mechanical properties of Sandvik 6C27 steel.

Mechanical property	**Value**
Yield stress	300 MPa
Young's modulus	210 GPa
Poisson ratio	0.3
Mass density	7.8 kg/m^3
Hardness	180-200 Vickers
Lankford coefficient for 0 °	1.3518
Lankford coefficient for 45 °	1.1763
Lankford coefficient for 90 °	1.8108

3.1.2 The Tensile Test Samples

Both the tensile test samples and the bend test samples where cut from a 0.5 mm thick strip. To study the plasticity the cross section of the rolling direction (RD), the normal direction (ND), was scanned.

The tensile tests were performed on a Zwick Z030. The machine was set to test until a certain plastic strain was reached. The tensile bars were stamped out from the strip. Tests were performed starting with 2% up to 24 % after which the material failed. In each test a new bar was used and the final strain was increased with 2%. Therefore one series consisted out of 12 bars. The procedure was repeated with a second set of bars for a repeat series. After the tests the samples were cut out of the center part of the bar in parts of 10 by 15 mm. (See Figure 15)

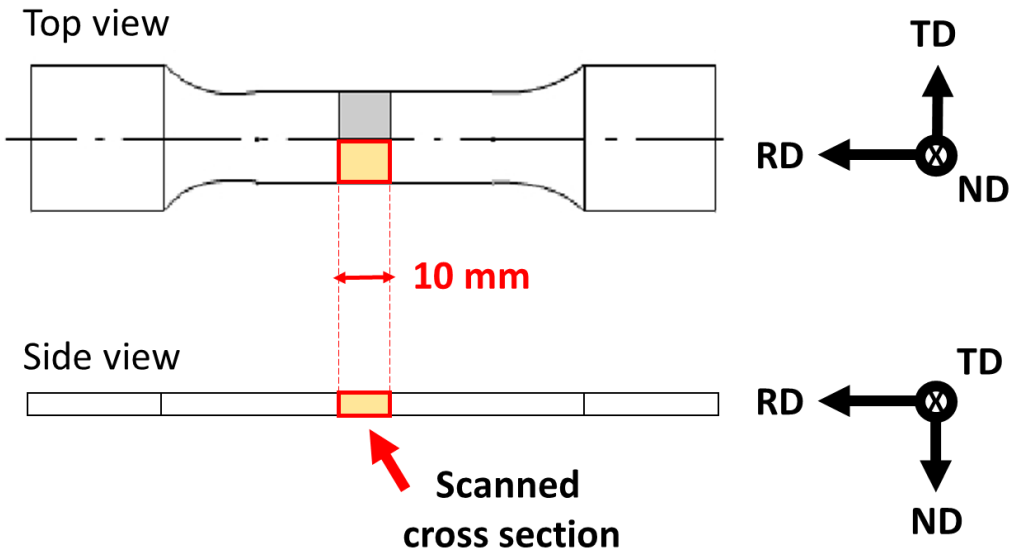

Figure 15 The EBSD sample (yellow) is cut out of the center part of the tensile test bar. The normal direction was scanned.

3.1.3 The Bend Test Samples

The bend samples were cut out of the strip as shown in Figure 16 and were bended with the Blech Tec BT150 bending machine. This machine clamps the sample at one side and bends the other side with a 2 mm thick rotating part. After the sample thickness and the bending angle is set and machine bends the sample automatically with a documented accuracy of 0.1 °. (See Figure 17)

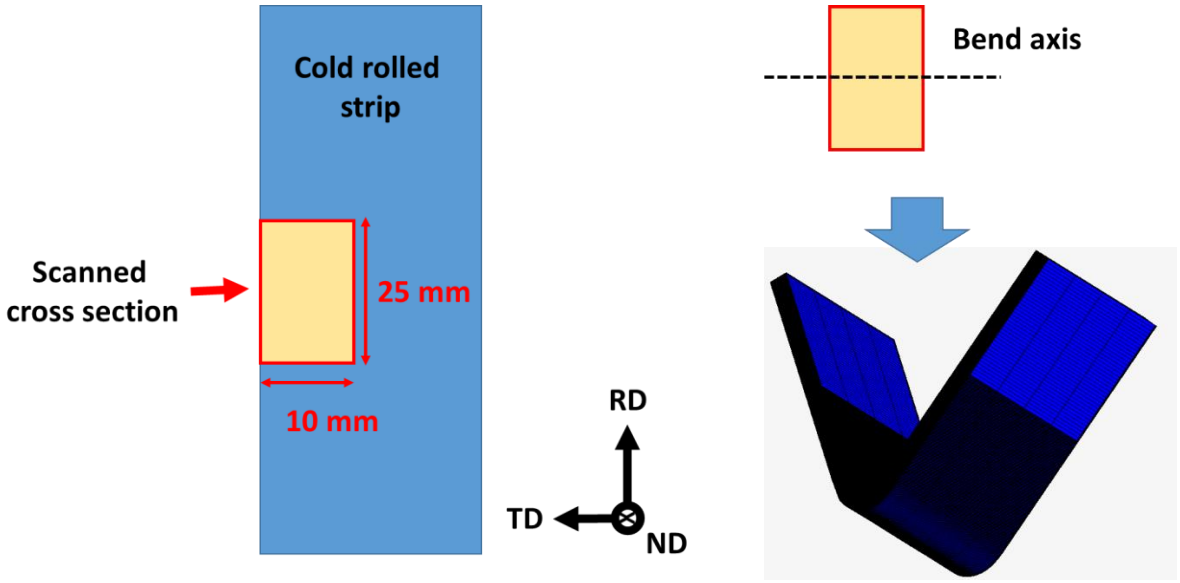

a b

Figure 16 An illustration of a) how the samples were cut from the strip and (in the case of the bend test) b) how they were bended.

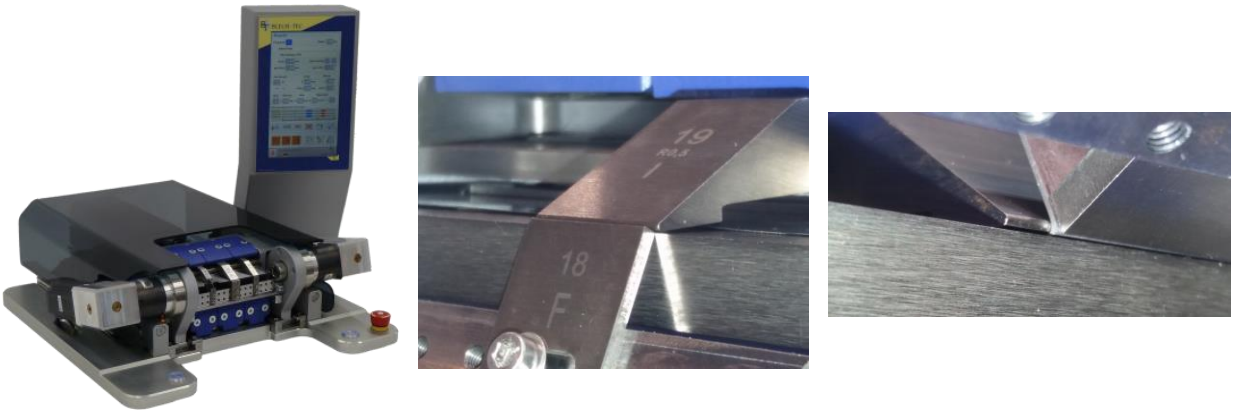

a b c

Figure 17 a) The Blech Tec BT150 bending machine, b) The sample is clamped between the nose tip. c) The sample is then bended over the 0.5 mm radius nose by a 2 mm thick rotating bending block.

Four angles were chosen to scan the misorientations in the normal direction of the sample. The resulting samples are illustrated in Figure 18.

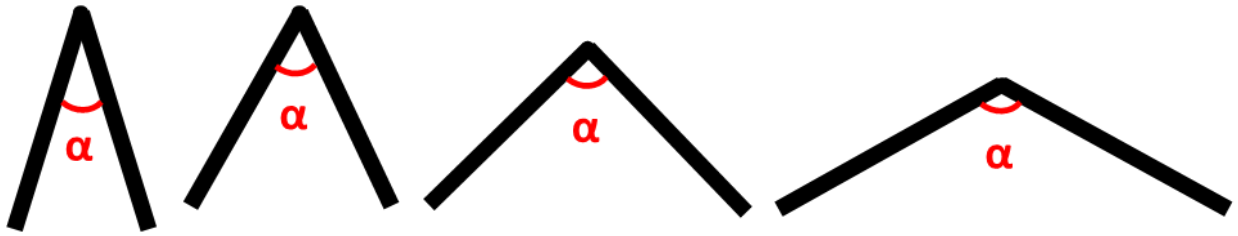

Figure 18 The four angles chosen for the bended samples.

The tensile test samples and bend test samples were cold mounted using nonconductive Demotec 33. They were grinded and polished using the steps in the order; sand paper, 9, 3 and 1 µm diamond particles suspension and finally 40 nm silica particles OPS suspension. The polishing times varied depending on the result. Finally the cold mounts were dissolved by placing them in a beaker with acetone and placing the beaker in an ultra-sonic bath. The dissolving procedure takes about a day in which the acetone needs to be refreshed every hour.

3.2 EBSD Hardware and Settings

For the EBSD scans a Philips/FEI XL30 ESEM FEG scanning electron microscope was used equipped with a TSL EBSD/OIM with DigiView 3 CCD camera. With the right settings this equipment can scan details of less than 100 nm in size. To study misorientations the scanned details have to be as small as possible. However these scans are lengthy in time and since this is a statistical study a tradeoff had to me made between the step size (as small as possible), binning size (as small as possible), the zoom factor ((>2000x is recommended) and the spot size (the current needs to be sufficient). Table 4 summarizes the used setting. With these settings an area of about 70x120 µm could be scanned in 16 hours.

Table 4 The EBSD settings used in this study.

Setting	**Value**
Acceleration voltage	25 kV
Spot size	5 (beam current about 2 nA)
SEM image zoom	800 – 1000 x
Binning of EBSD CCD camera image	2x2 (624x468)
Frame rate	20 fps
Step size in hexagonal grid	0.1 µm

3.3 The Orowan's Model for an Hexagonal Grid Scan

In the theory chapter a simplified dislocation density model using the misorientations between pixels and Orowan's formula were explained. Each EBSD scan discussed in this study is processed using this approach. This section explains the details with which it was implemented.

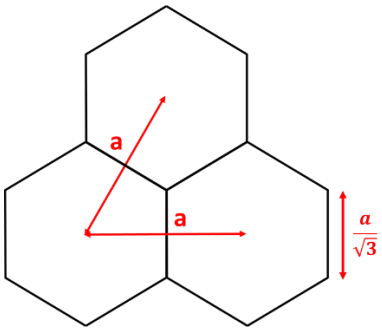

Figure 19 an example of the hexagonal grid used with step size a. One hexagonal is one pixel in the scan.

For this study a hexagonal grid rather than a squared grid was used. This alters the equations for the dislocation density. One pixel faces 6 other pixels instead of 4 and the length of one border is $\frac{a}{\sqrt{3}}$ instead of a with a being the step size of the scan. The surface of a hexagonal pixel is $\frac{a^2\sqrt{3}}{2}$ instead of a^2. Figure 19 shows an example of 3 neighboring pixels.

With these changes the number of dislocation along one border becomes:

$$n_{dislocation} = \frac{a}{\sqrt{3}}\frac{\phi}{|b|} = \frac{a}{\sqrt{3}}\frac{\theta_{mis}}{2|b|} \tag{14}$$

The dislocation density of one pixel (with 6 borders) becomes:

$$\rho_{pixel} = 6\ \frac{a}{\sqrt{3}}\frac{\theta_{mis}}{2|b|}\frac{2}{a^2\sqrt{3}} = \frac{2\,\theta_{mis}}{a|b|} \tag{15}$$

This equation is suitable when taking the average misorientation of all six borders. The misorientation treatment used for this approach is the kernel average misorientation level 1 (**KAM 1**). This is used in Orowan's equation together with D_{travel} as the mean distance the dislocations have travelled during the plastic deformation. Furthermore the orientations of the grains influence the degree with which they deform. Therefore the calculated microscopic plastic strain of each pixel is weighted with the Schmid factor of the grain it belongs to. Inserting all in Orowan's equation gives the microscopic plastic strain used in this study:

$$\varepsilon_{p,micro} = |b|\,\rho_{pixel}\,D_{travel}\,\frac{1}{2SF} = |b|\,\frac{2\,\theta_{mis}}{a|b|}\,D_{travel}\,\frac{1}{2SF} = \frac{2\,\theta_{mis}\,D_{travel}}{a\,2SF} \tag{16}$$

In each EBSD scan the grain shapes are logged and used to estimate D_{travel}. The grain shape is rotated until its length lies parallel with the horizontal axis, then an ellipse fit is performed. The mean of the semi minor and semi major axes is taken as the traveled distance. Figure 20 shows the principle of this technique.

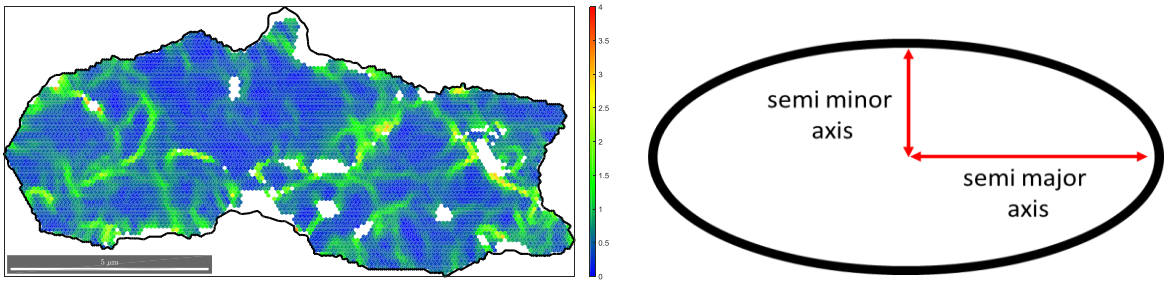

a b

Figure 20 a) A KAM 1 image of a grain (24 % plastic strain) b) An example of an ellipse fit where the average of the two axes is taken as an estimate for the travelled distance of the dislocations in this grain.

The microscopic plastic strain of each pixel is calculated using D_{travel} and the Schmid factor of the grain it belongs to. The algorithms for the data processing and the plotting of the results were programmed in Matlab 2016b (Mathworks). The orientation data was calculated using the open source MTEX 5.0.3 package.

3.4 Plotting

The results are presented in tow different formats depending on the purpose. The tensilte test samples were assumed to have homogeneous plastic strain. Therefore the mean and standard deviation of the microscopic plastic strain of the whole scan was taken as a data point. The results of the bended samples are presented as mean values of each grain projected in a graph with the corresponding average y coordinates of the grains. Figure 21 shows an example of how a scan is perfomed and Figure 22 shows how this scan (rotated 90 ° in this Figure) is plotted after it has been processed.

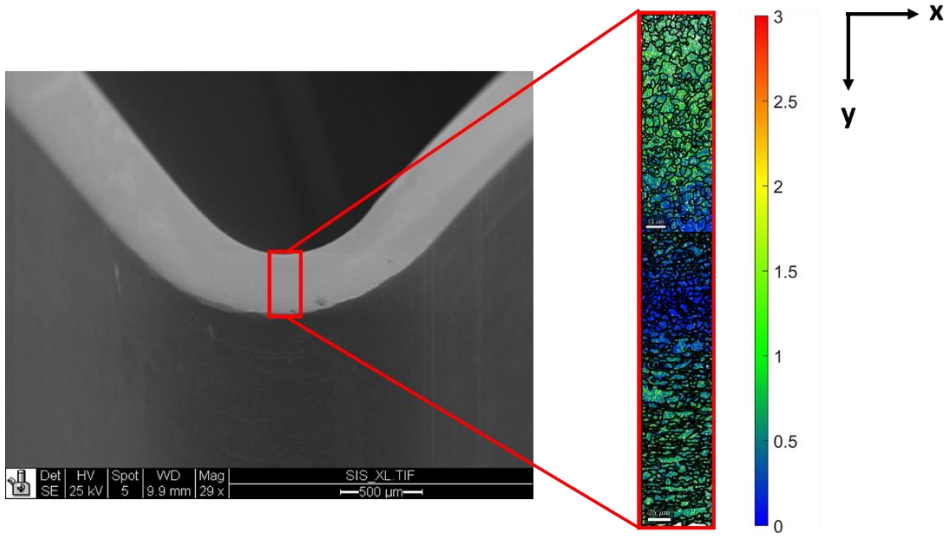

Figure 21 An example of an EBSD local misorientation map (right) from the scan performed on the scross section of a bent sample shown in the SEM image (left).

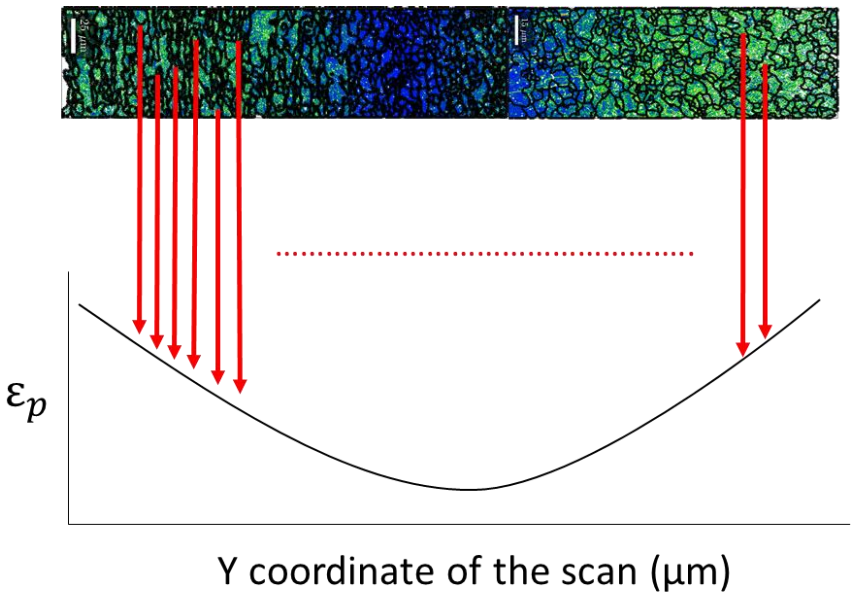

Figure 22 An illustration of how the results of the EBSD scans of the bent samples are presented. The mean value of each grain is projected as a line with the corresponding y coordinates.

3.5 The FEM Calculations

The finite element modelling (FEM) was done using Marc Mentat 2017 (MSC) using a material model set up with in-house mechanical property measurements of Sandvik 6C27. These properties can be found in Table 3 of this chapter. The FEM is a model of the bending mechanism of the BT150 bending machine and is shown in Figure 23.

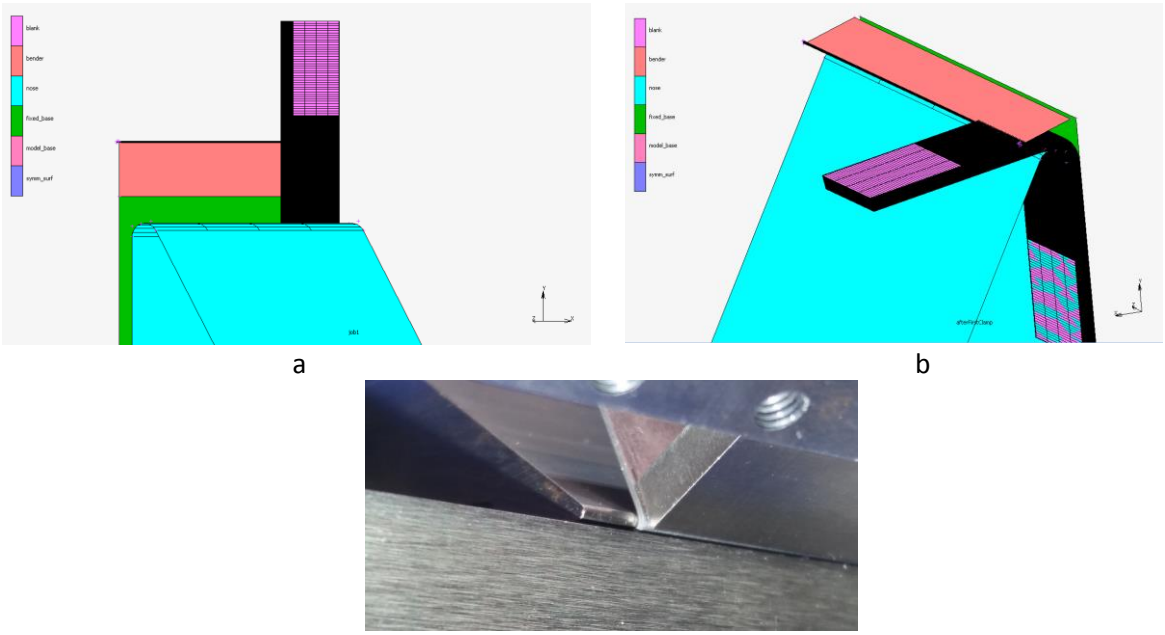

a b

c

Figure 23 The FEM of the bending machine a) Starting point. b) Bending. c) The actual machine that is bending.

The model blank was 10x15 mm by 0.2 or 0.5 mm thickness and was build up in three parts. The two outer parts contained fewer elements. The middle part formed the tip of the bending. The elements in the cross section (y and z dimension) of the middle part of the blank were 10x15 µm which corresponds with the average grain size of the used material (~10x~10 µm). Table 5 shows an overview of the elements in the blank.

Table 5. The number of elements used in half of the blank.

	X dimension 0.2 mm	X dimension 0.5mm	Y dimension	Z dimension
Upper part	20	50	40	4
Middle part	20	50	540	4
Lower part	20	50	40	4

The settings were tuned by comparing the bend angles and the tip shape with measurements of the actual samples. Figure 24 shows an end result for the 60 ° bend sample.

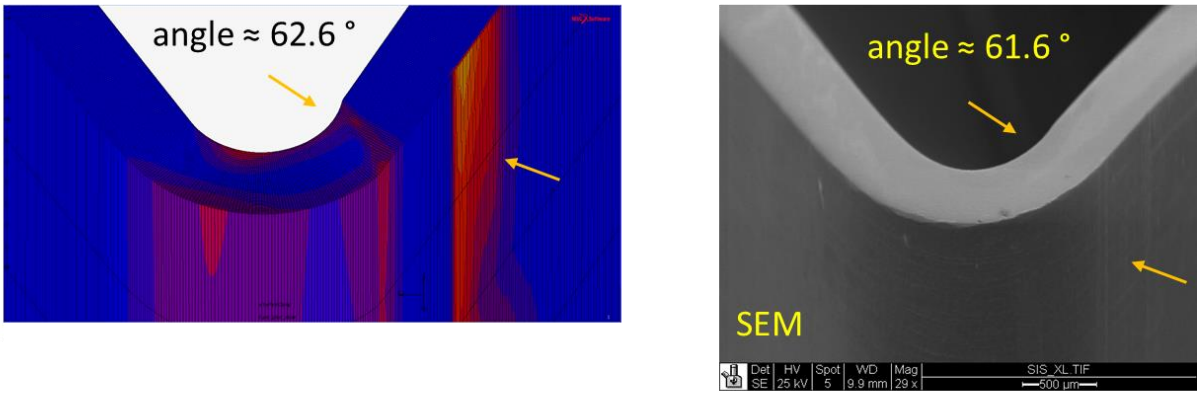

Figure 24 A comparison between the FEM (left) model and the SEM image (right) of the 60 ° bend sample. The compression and the friction damage of the bender are indicated with the arrows..

After running the model the nodes and mechanical values of each node were loaded in Matlab. Since the EBSD scans had dimensions of about 70x500 µm, an area of nodes was taken as the cross section values rather than a line of nodes. Figure 25 shows these areas for different locations on the tip of the sample. The distances between the center points of the areas A-B, A-C and A-D are 180 µm, 400 µm and 240 µm respectively. This way of defining the positions is independent of the sample thickness. The algorithm that extracts the nodes at these positions also calculates the angle of area with respect to the horizontal direction.

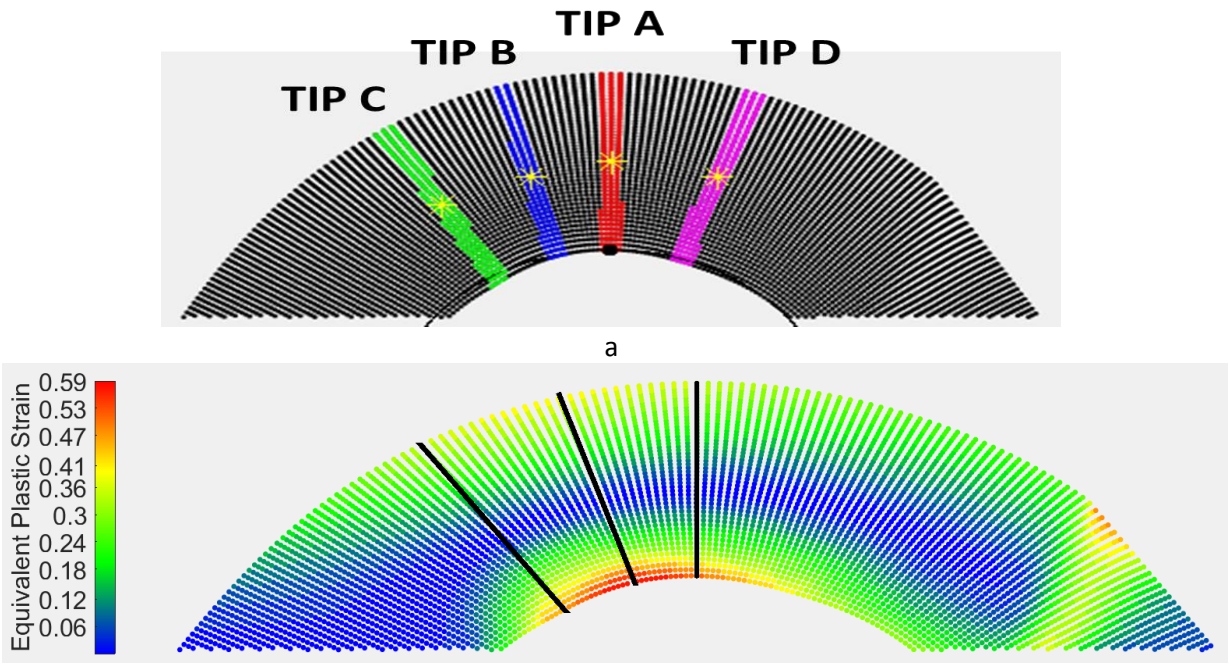

Figure 25 The FEM results extracted in Matlab. a) The node coordinates with the selected areas for the cross sections. b) The plastic strain values for each node with tip A, B and C indicated.

3.6 The Gage R&R

To investigate the reliability of the EBSD in characterization of local strain a gage repeatability and reproducibility (gage R&R) test was performed. When an EBSD measurement is repeated with the same sample different outcomes can be expected because of procedure spread. This spread is an accumulation of sub spreads that are introduced by the different factors that play a role during the measurement. Table 6 gives a selection of some possible spread sources. A series of scans is performed in which every setting of one factor is tested while keeping the rest of the factors and settings the same. Each of the combinations is repeated three times to test the repeatability. This technique identifies the spread introduced by each factor used in the test by analyzing the data with an analysis of variances (ANOVA). Figure 26 shows an overview of this technique using only one factor. With each factor the test becomes larger. For this study only one factor was used which is the reloading of the sample and the tuning of the beam. The settings used in this study (See table 4) were used and kept constant throughout the test. A sample was loaded, the beam was tuned and the same 25 x 25 µm area was scanned three times without turning off the beam between scans. Then the sample was unloaded and the procedure was repeated another two times for the same area. This resulted in a data set of nine scans of the same area. From these scans the common grains that were completely in the area were selected to be processed. The KAM and the MORI calculations were performed for each of these grains resulting in a set of mean values for each grain. These mean values were then used in the ANOVA.

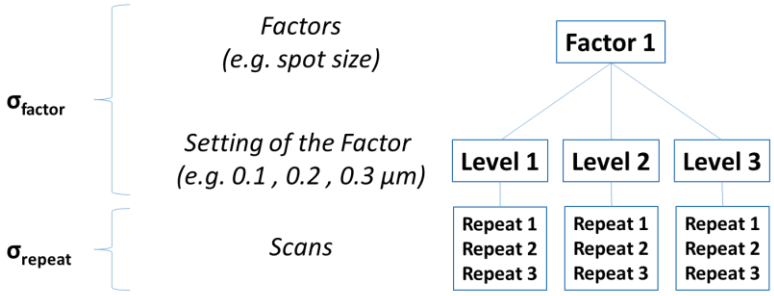

$$\sigma_{total} = \sqrt{\sigma_{factor}^2 + \sigma_{repeat}^2}$$

Figure 26 A schematic overview of a gage R&R with one factor and the sub spreads σ.

Equation 17 is the formula used for this one factor ANOVA. One scan result (y_{ij}) is made up of the mean scan result ($\bar{y}$), the contribution of the factor spread (α_j) and the residual error from the repeatability (ε_{ij}). The indices j and i refer to the factor and the repeat within one factor respectively.

$$y_{ij} = \bar{y} + \alpha_j + \varepsilon_{ij} \tag{17}$$

Table 6. A selection of the possible spread sources during an EBSD scan.

Factor	**Influence**	**Used in the gage R&R**
Operator	Between operators	Not used
Loading and beam tuning	Operator	**Used**
Sample material	Difficulty of crystal structure detection	Not used
Scan area in the SEM image	Fish eye effect (the best scan is in the middle of the image)	Not used
Acceleration voltage	Resolution	Not used
Spot size	Resolution	Not used
Zoom	Resolution	Not used
Binning	Resolution	Not used
Frame rate	Resolution	Not used
Step size	Resolution	Not used

4 Results and Discussion

In this chapter first a microstructure and texture overview of the used material is given. Then the results of the correlation between the misorientaions and the macroscopic plastic strain using the tensile tests will be shown and discussed. After that the implementation of this correlation in the bend tests and its agreement with the finite element model calculations will be presented. Finally the reliability of the scans are discussed with the results of the gage repeat and reproducibility tests. The EBSD data of each scan discussed in this chapter was processed two times. Table 7 explains the two treatments of the misorientation data of the scans.

Table 7 The treatments of the misorientations of this study.

Treatment	**Description**
Using the KAM 1 data	The correlation of the KAM 1 misorientation and the macroscopic plastic strain. The KAM is calculated for the nearest pixel neighbor and the average of all the KAM values in a grain is taken.
Using the MORI data	The correlation of the MORI misorientation and the macroscopic plastic strain. The MORI is the misorientation value of each pixel in a grain with respect to the mean orientation of that grain. Then the average of all these values in a grain is taken.

4.1 The microstructure of an undeformed sample

An EBSD scan of the undeformed material was done to estimate the offset for the tensile test correlation. This sample was labeled '0 % strain'. Figure 27 shows the statistical data of this scan. The grain diameters are estimated by fitting an ellipse on a grain and by taking the mean of the minor and major axes. It is the same procedure with which the dislocation travel distance is estimated. In Figure 27 this distance is multiplied by two. The majority of these scanned grains have an estimated grain diameter of about 3 microns. There are however a substantial number of larger grains with diameters up to 12 microns. Also shown is the distribution of the KAM 1 values. At this undeformed state these values are about 0.1 degrees.

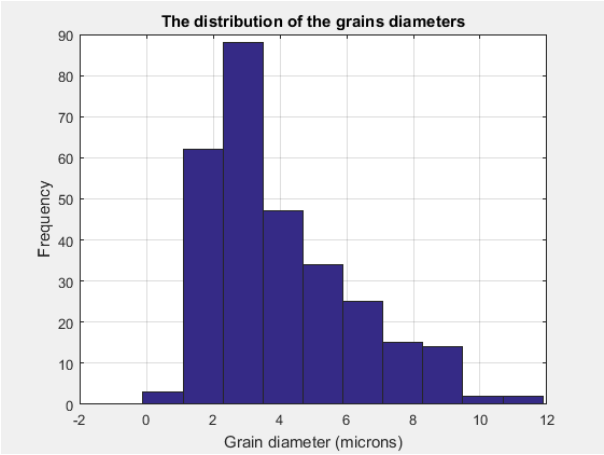

a

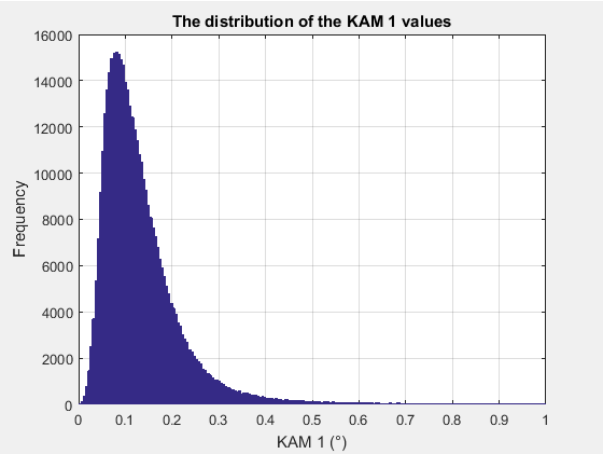

b

Figure 27 The statistical data of the scan of the undeformed sample with a) the distribution of the estimated grain diameters and b) the distribution of the misorientation data.

Figure 28 shows the inverse pole figure ([0 0 1]) of the scan. The map shows no clear preference in direction.

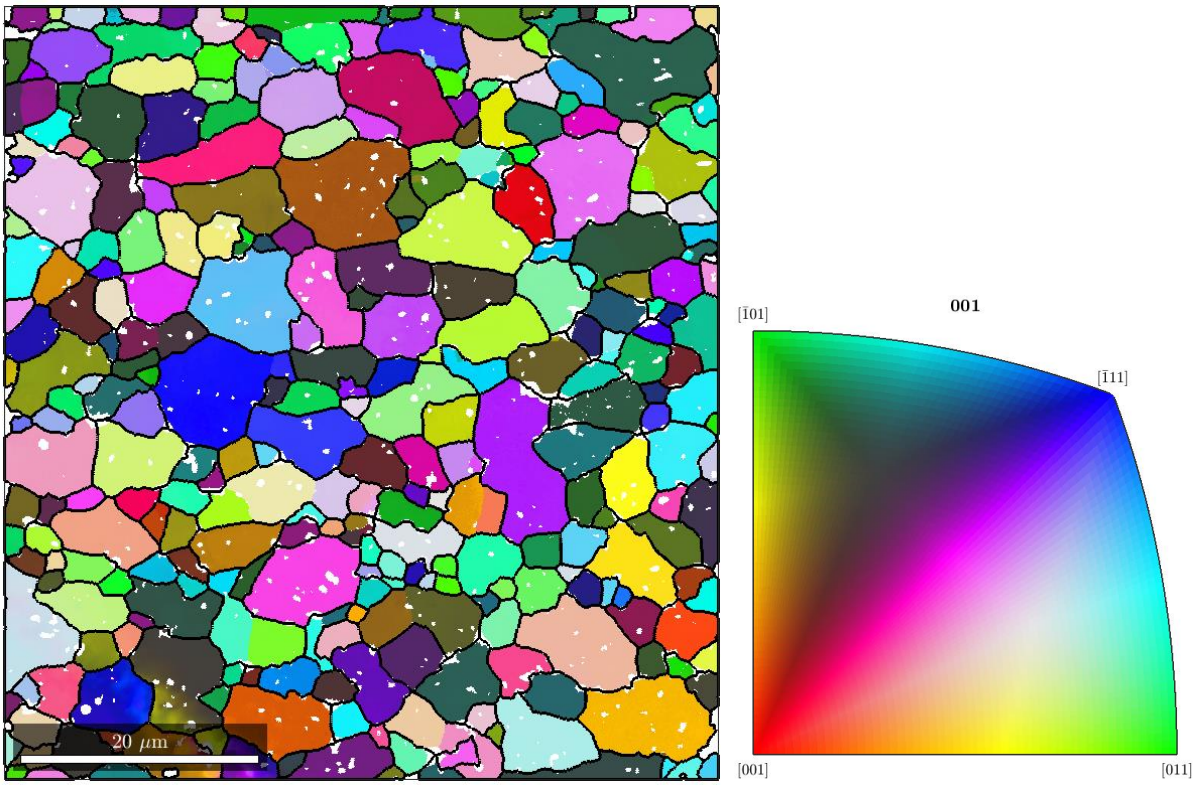

Figure 28 [0 0 1] inverse pole figure map of the undeformed sample.

4.2 The Tensile Tests Results

Tensile tests were performed starting with 2% up to 20 % strain after which the material started to fail. The samples were cold mounted and polished. EBSD scans were made at the side of the sample (normal direction) as illustrated in Figure 15. The edges of the samples were omitted and only the center region was scanned. Figure 29 shows the KAM 1 maps of the scans that were used. A clear increase in local misorientations due to the plastic strain introduced by the tensile test is visible.

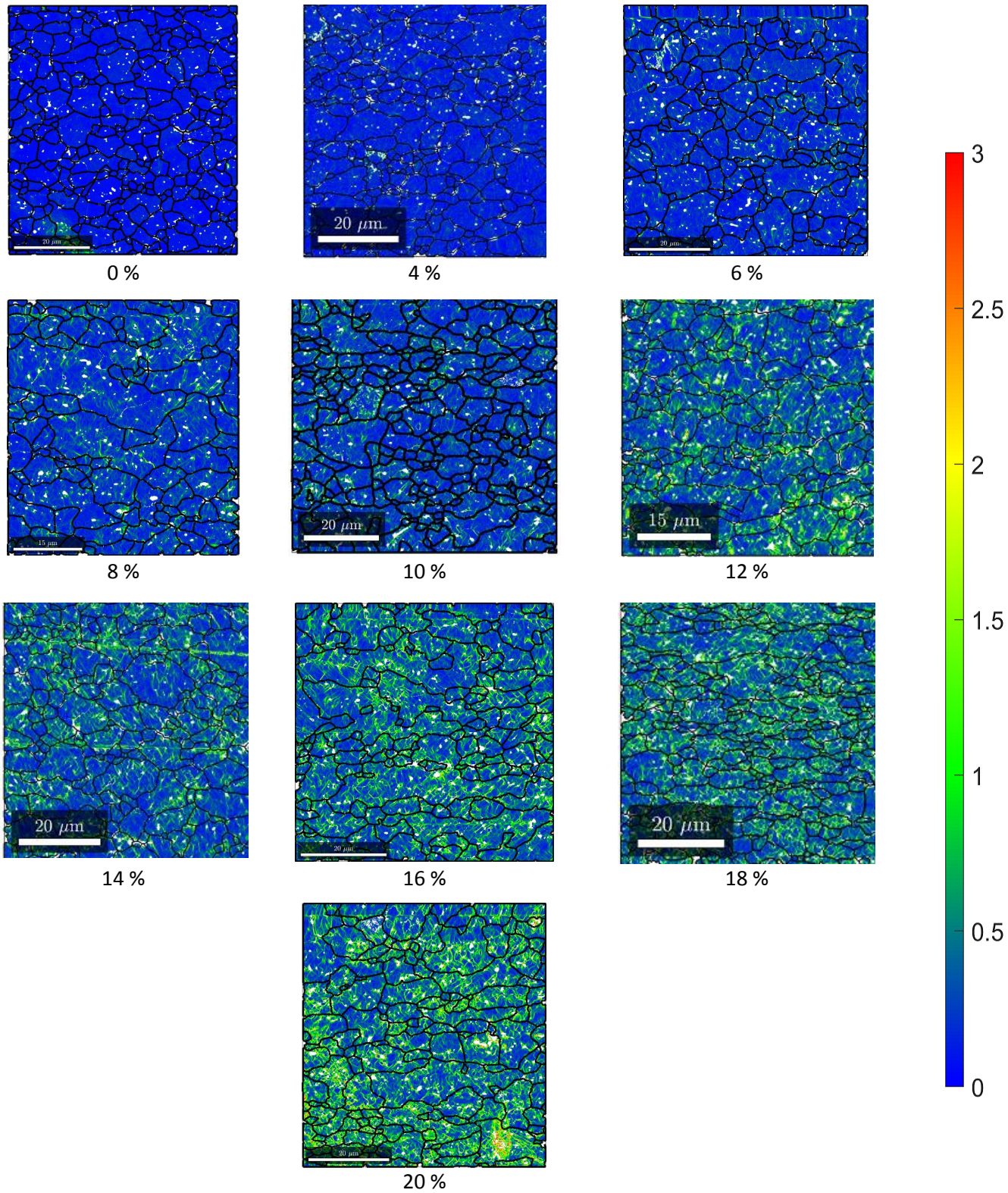

Figure 29 KAM1 maps for tensile samples strained up to indicated value of plastic strain. The threshold for the grain boundaries is 10 ° and is used for every scan in this study. On the right the misorientation scale bar (in °) is shown.

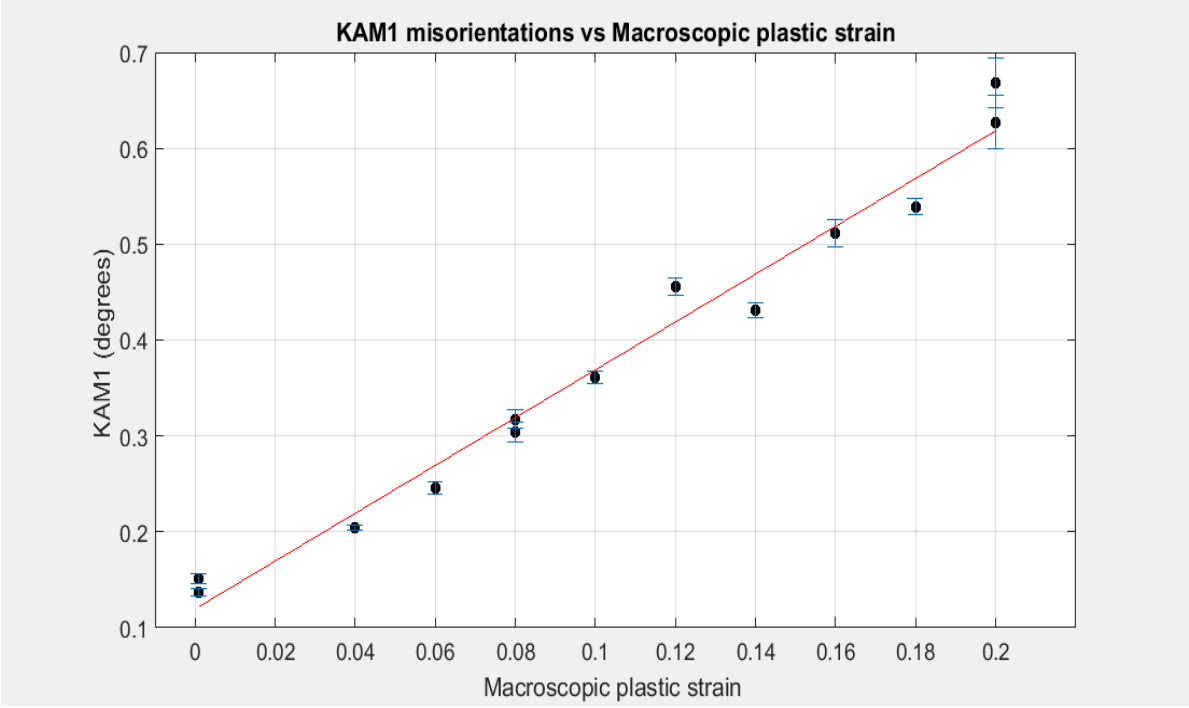

a

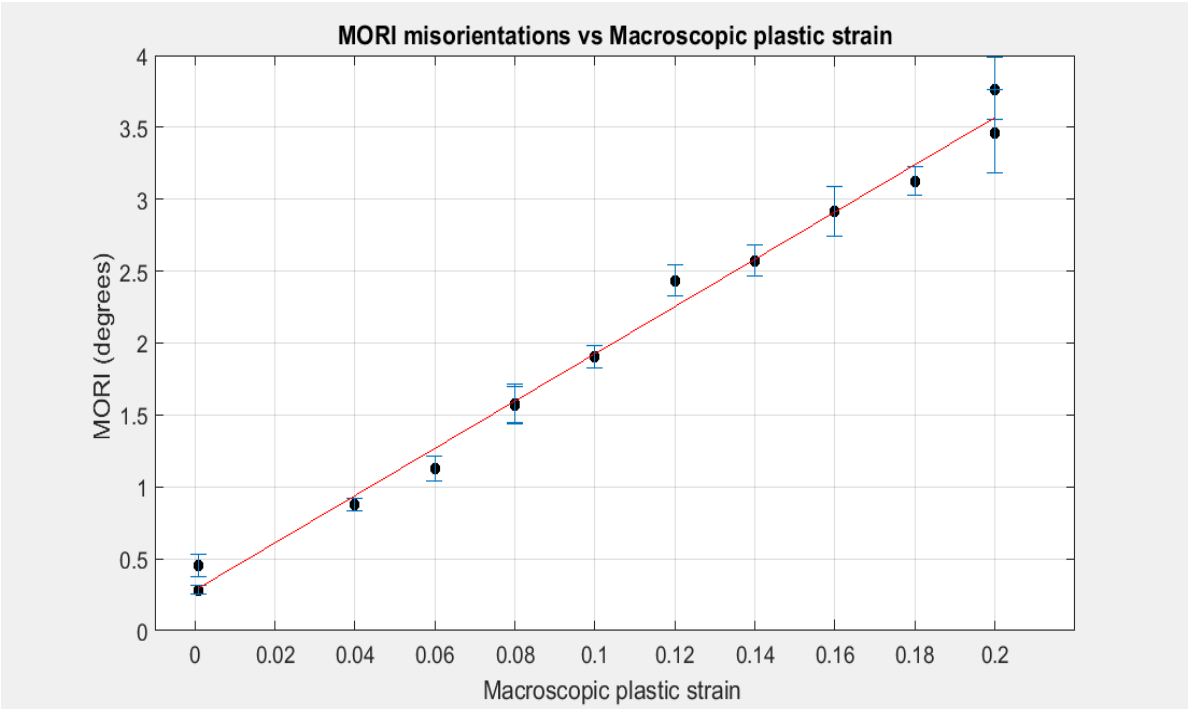

b

Figure 30 The mean grain value correlations with the tensile test plastic strains. Here the data was calculated using the mean grain values of each scan. a) The correlation of the KAM 1 misorientation data with the plastic strain. b) The correlation of the MORI misorientation data with the plastic strain..

Two correlations were studied. These are shown in Figure 30. The first is that of the KAM 1 misorientations angles and the macroscopic plastic strain and the second is that of the MORI misorientations angles and the macroscopic plastic strain. Table 8 shows the correlation equations and the statistics. The offsets agree very well with the data obtained from the undeformed samples that were shown in Figures 28 and 29a. The confidence interval data shows that the slope is significantly larger than zero. There clearly is a strong relation between the misorientations and the macroscopic plastic strain applied with the tensile tests. Because of limited time the tensile test scans were done for a limited area. The tensile tests should be repeated and more scans of each sample should be done. Table 9 shows the areas and number of grain used in each scan. Nevertheless the correlation is very clear.

Table 8 The correlation equations and the statistics of Figure 30.

Used data set	**Correlation equation**	**R^2**	**The 95 % confidence interval of the offset**	**The 95 % confidence interval of the slope**
KAM 1 misorientations vs Macroscopic plastic strain	$\theta_{mis} = 0{,}1195 + 2{,}4947 * \varepsilon_{p,macro}$	0,977	Lower: 0,0969 Upper: 0,1383	Lower: 2,1296 Upper: 2,4629
MORI misorientations vs Macroscopic plastic strain	$\theta_{mis} = 0{,}2815 + 16{,}4358 * \varepsilon_{p,macro}$	0,991	Lower: 5,7519 Upper: 12,9090	Lower: 212,7233 Upper: 270,4251

Table 9 The areas and number of grains used in the tensile test correlation.

Macroscopic plastic strain (%)	**Scanned area (µm x µm)**	**Number of grains**
0	60x64	260
4	65x160	511
6	60x62	157
8 b (copy series)	45x45	89
8	50x55	102
12	55x140	319
14	65x160	365
16	60x60	137
18	62x180	548
20	60x65	143
20 (another scan, same sample)	40x40	52

Figure 31 shows the results of the attempt to calculate the microscopic plastic strain using the simplification that assumes all misorientations are the direct cause of glide dislocations. This crude model was used in Orowan's equation, together with a rough estimate of the dislocation traveling distance and the Schmid factor. The microscopic plastic strain values (y axis) are clearly too high. Values in the order of 10^{-1} were expected instead of values of the order of 10^{1}. The order of magnitude can be explained by the number of dislocations counted in each pixel as described in Figure 14. Since the KAM 1 misorientation does not exceed 5 °, the number of dislocations in each pixel of the scan will be too high. Furthermore, misorientations are not caused by glide dislocations only and it is very challenging to recognize what combination of dislocation types caused a misorientation. Needless to say, this model clearly does not translate misorientations in microscopic plastic strain in the correct manner. The correlation in Figure 31 exists because of the indirect relation of misorientation in the dislocation model used. This can be expected because

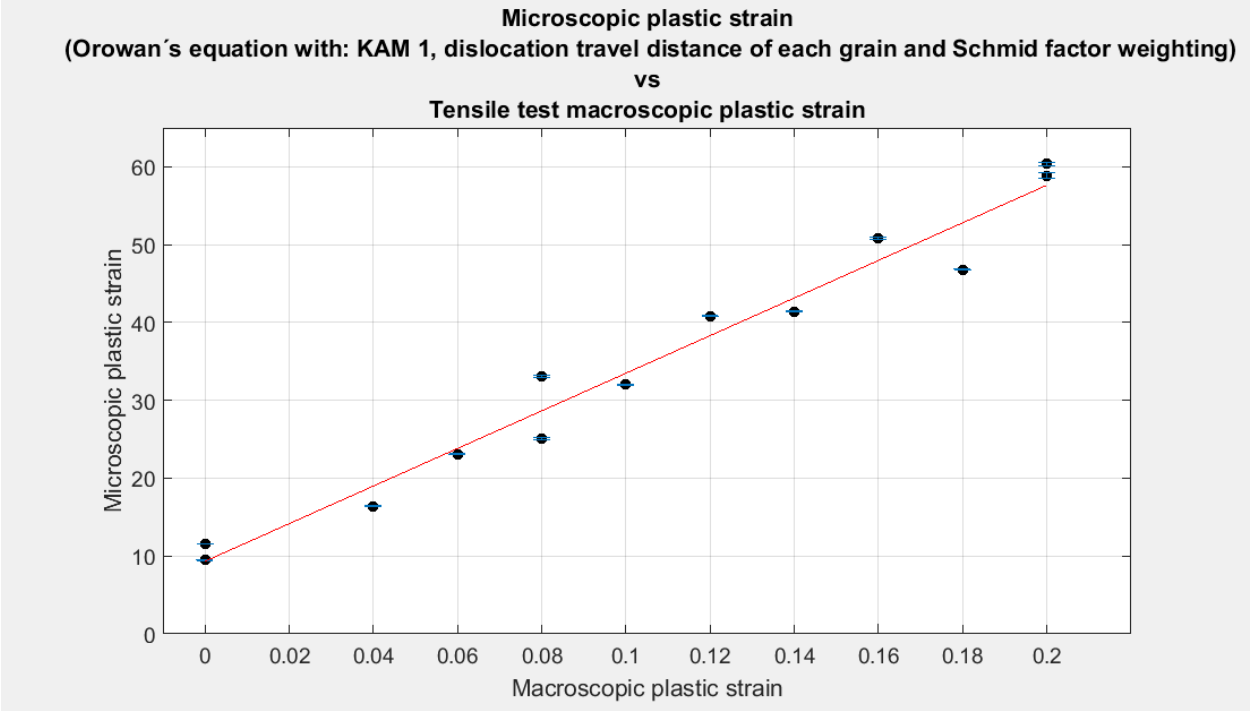

Figure 31 The correlation of the data derived using Orowan's equation and the KAM 1 misorientation data, and the macroscopic plastic strain values from the tensile tests. The pixel value correlations with the tensile test plastic strains.

4.3 The Bend Test Results

In this paragraph the implementation of the correlations in the bend test scans are presented. This is done for the cold mounted samples and for the hot mounted samples.

4.3.1 The Cold Mounted Samples

In this section the macroscopic plastic strain derivations of bent samples are presented. Of each measurement result two plots are shown. The first is the misorientation data and the equivalent plastic strain data from the FEM computation. In the second plot the correlation relation of the misorientation data with the tensile test plastic strain data is used to calculate the macroscopic plastic strain. The result is plotted together with the equivalent plastic strain data from the FEM computation. Both results are smoothened with a convolution filter with a kernel of n = 100.

Figure 32 shows the results for the 40° cold mounted bended sample. The two curves are very similar in shape and agree well with the FEM data except at the edges of the sample.

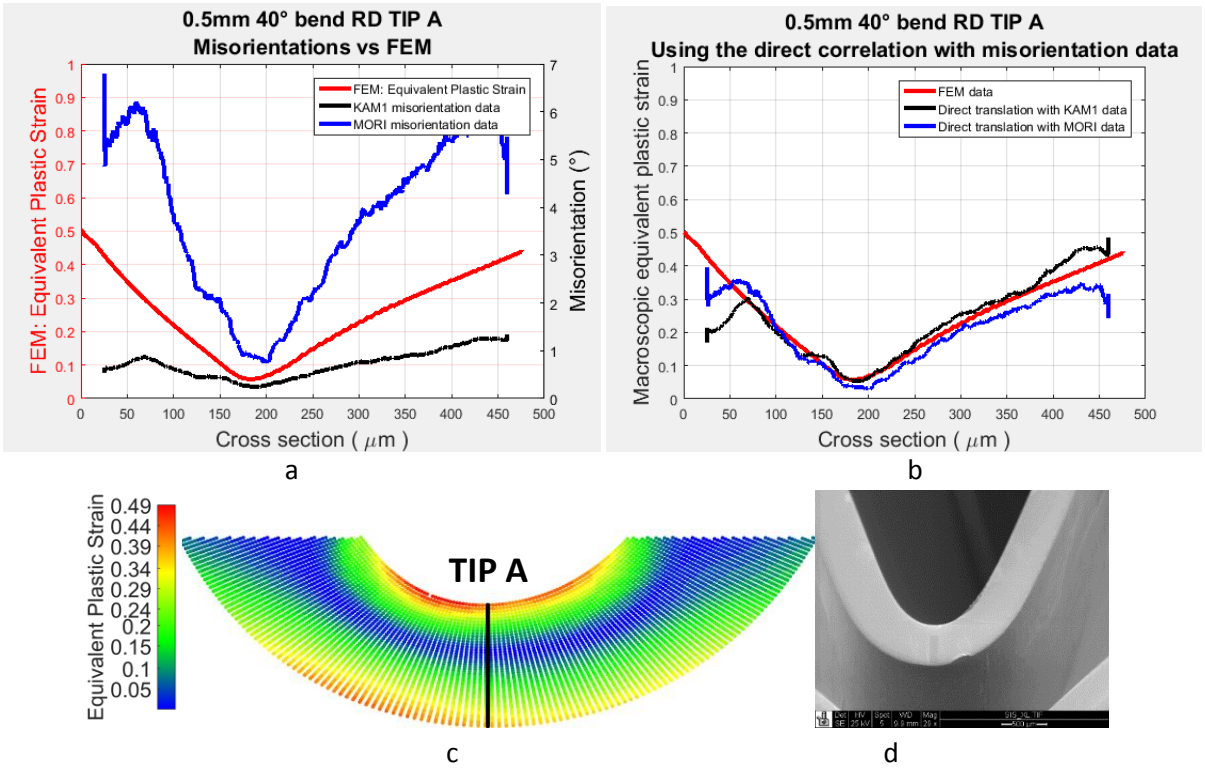

Figure 32 The results of TIP A of the 40° 0.5 mm thick bent sample. The red line is the FEM data. a) The misorientation data and the FEM data plotted with separate y axes. b) ε_p derived with the misorientation and macroscopic plastic strain correlation plotted together with the FEM data. c) The FEM results of ε_p. d) The SEM image of the sample.

Near the edges of the sample the local misorientation data deviate or is missing. This is due to difficulty of indexing of the EBSD signal because of the rounding of the edges during polishing or due the extreme deformation (> 35 %) in these areas. Figure 33 shows the KAM 1 map of the top part of the EBSD scan. It is clear how the misorientation density increases towards the upper edge of the figure and how eventually more and more pixels could not be reliable indexed (Confidence index < 0.1). These data vacancies are white in the image. Therefore parts close to the edges tend not to agree well with the FEM data. The spikes at the edges of Figure 32b could be explained with the influence of the grain size. Figure 34 shows an example of a very large grain in this part of the scan. Since the data is plotted with the mean values of each grain, this could have caused a larger data point value. For this reason scans of more copies of this sample should average out these spikes.

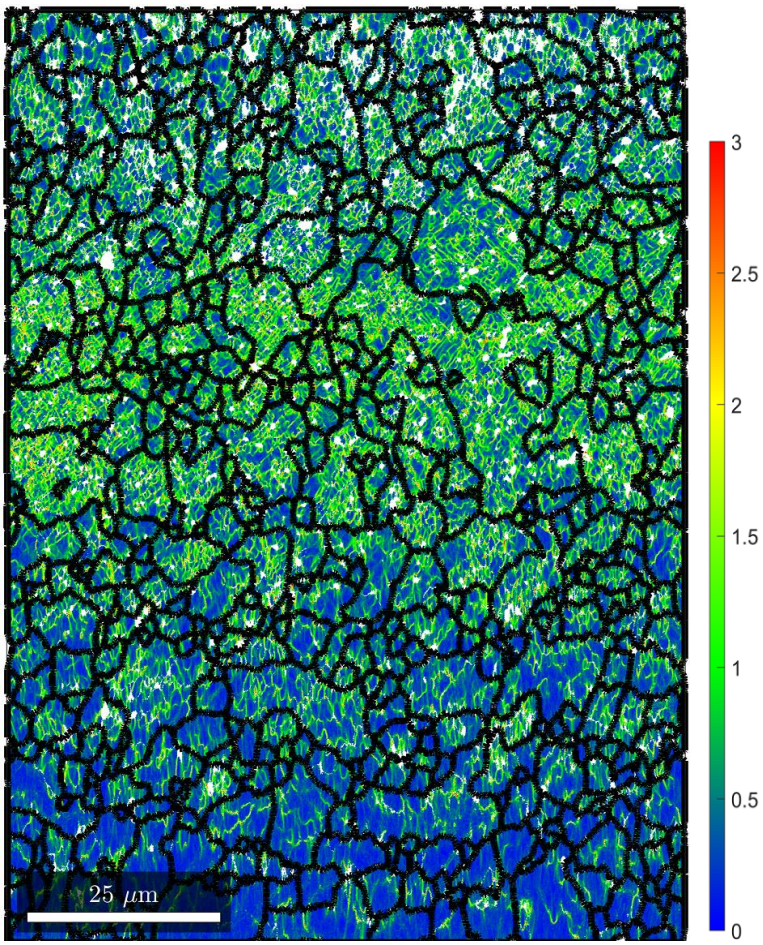

Figure 33 The KAM 1 map of the first part of the 40 ° bent sample scan. Towards the edge (upper side) the misorientation density increases and eventually bad indexing starts to occur (white regions).

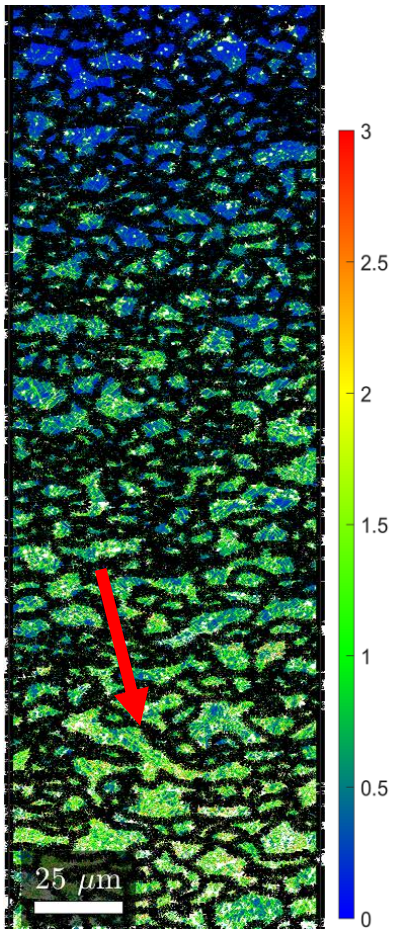

Figure 34 The KAM 1 image of the last 200 µm of the TIP A 40° bent sample scan. A large grain could cause a spike.

Figure 35 shows the TIP A and TIP C results of the 60° cold mounted bended sample. The results of TIP A shows a poor fit with agreement with the FEM results. This was the only scan that had a poor agreement and it is not clear why the misorientation values increase rapidly at 150 and 300 µm. The results of TIP C shows a good agreement with the FEM data apart from a slight deviation on the left side.

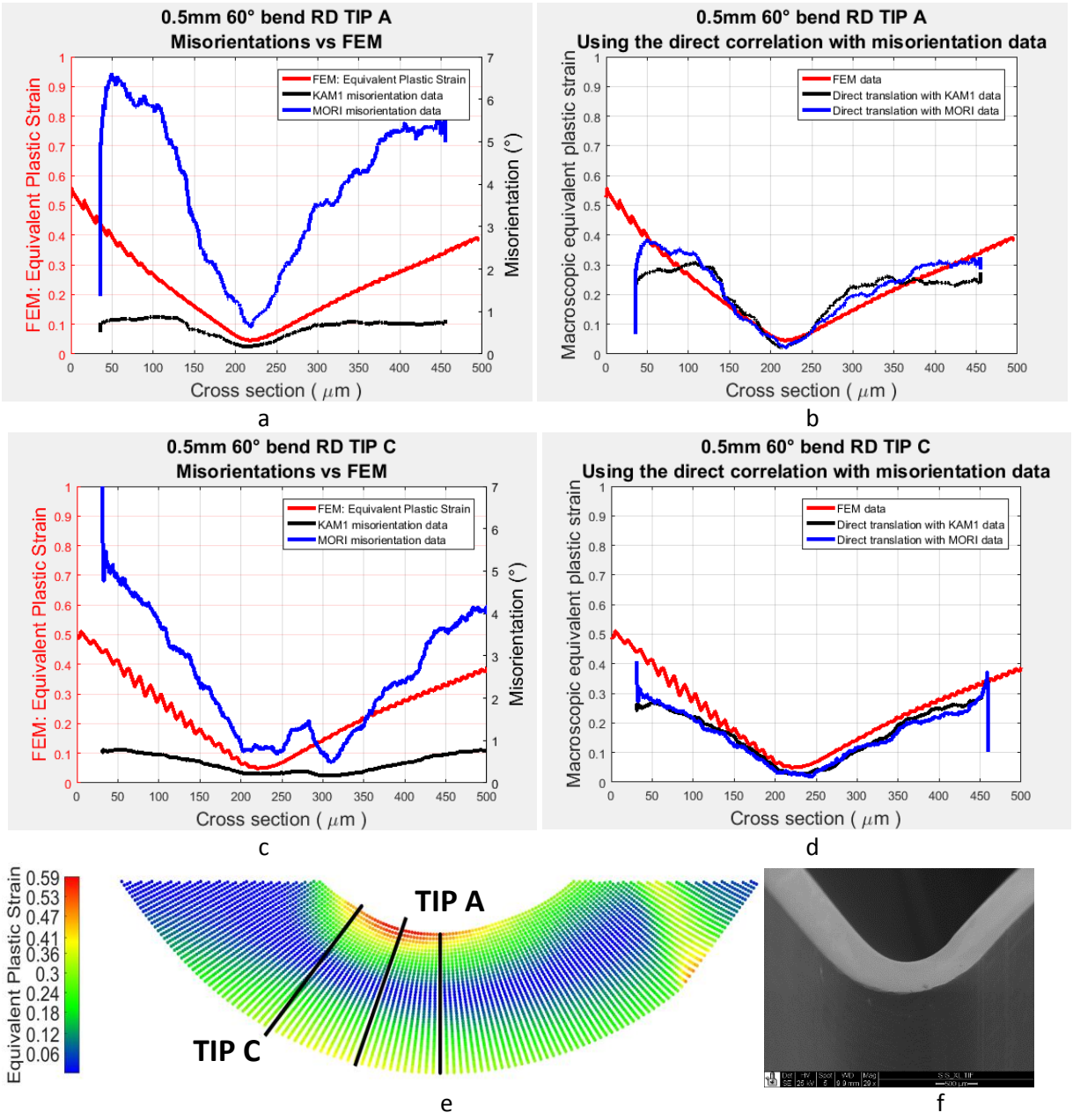

Figure 35 The results of TIP A and TIP C of the 60° 0.5 mm thick bent sample. The red line is the FEM data. a) TIP A: The misorientation data and the FEM data plotted with separate y axes. b) TIP A: ε_p derived with the misorientation and macroscopic plastic strain correlation plotted together with the FEM data. c) TIP C: The misorientation data and the FEM data plotted with separate y axes. d) TIP C: ε_p derived with the misorientation and macroscopic plastic strain correlation plotted together with the FEM data. e) The FEM results of ε_p. f) The SEM image of the sample.

Figure 36 shows the TIP A results of the 90° cold mounted bent. Due to rounding off of the edge the first 50 µm could not be scanned. The results agree very well with the FEM data. The slopes in Figure 36b follow the FEM data accurately.

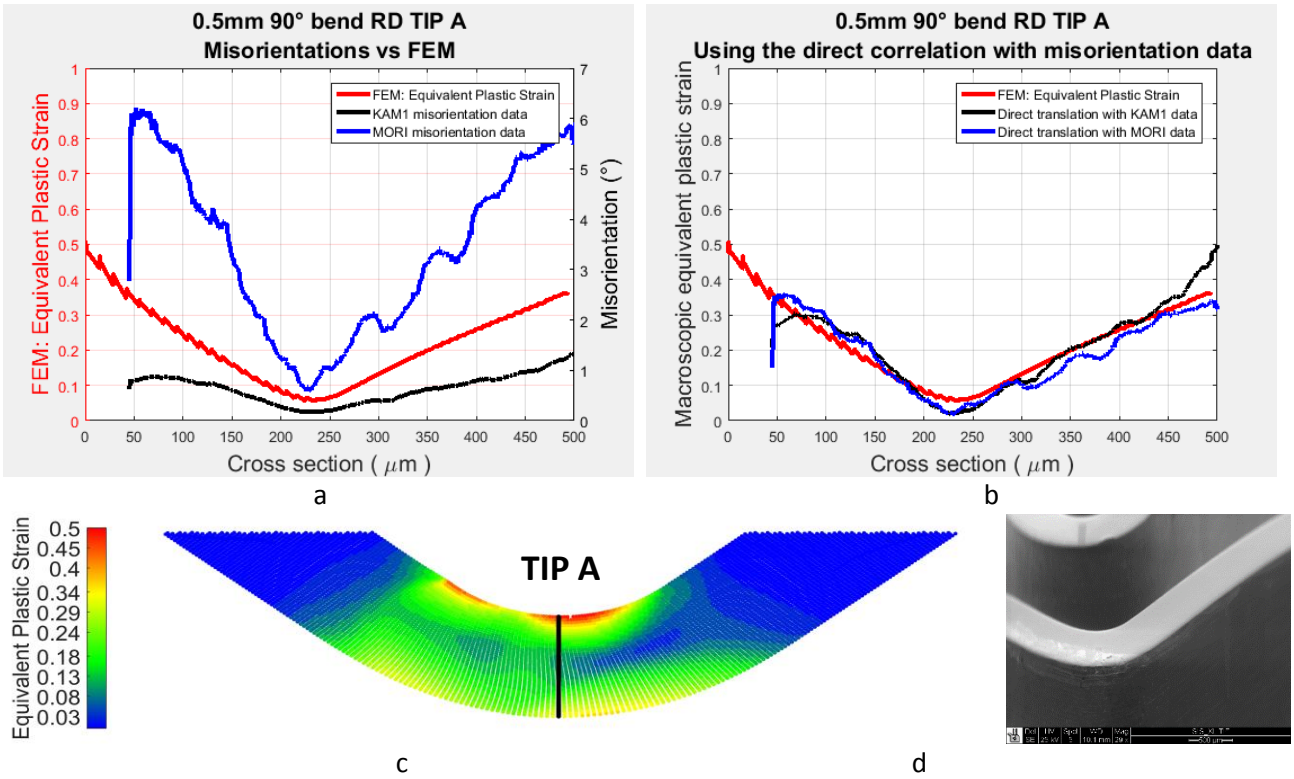

Figure 36 The results of TIP A and TIP C of the 90° 0.5 mm thick bent sample. The red line is the FEM data. a) TIP A: The misorientation data and the FEM data plotted with separate y axes. b) TIP A: ε_p derived with the misorientation and macroscopic plastic strain correlation plotted together with the FEM data. c) The FEM results of ε_p. d) The SEM image of the sample.

Figure 37 shows the TIP B and TIP C results of the 135° cold mounted bent sample. The FEM values of this angle were considerably lower than in previous samples. The correlations agree fairly well apart from a few deviations. After inspection the spikes at 350 µm of TIP B and at 70 µm of TIP C were caused by exceptional high misorientation densities that were very local. This is shown in Figure 38 and 39.

The results of these scans show a typical deviation from the FEM data that is visible in the results of all samples discussed. The low plastic strain values do not agree well with the FEM data. In those regions the data derived from the scan contains about the same values of misorientations as seen in undeformed samples. This translates into ~0 % strain. However the FEM calculation rarely shows 0 % strain in the center of the sample.

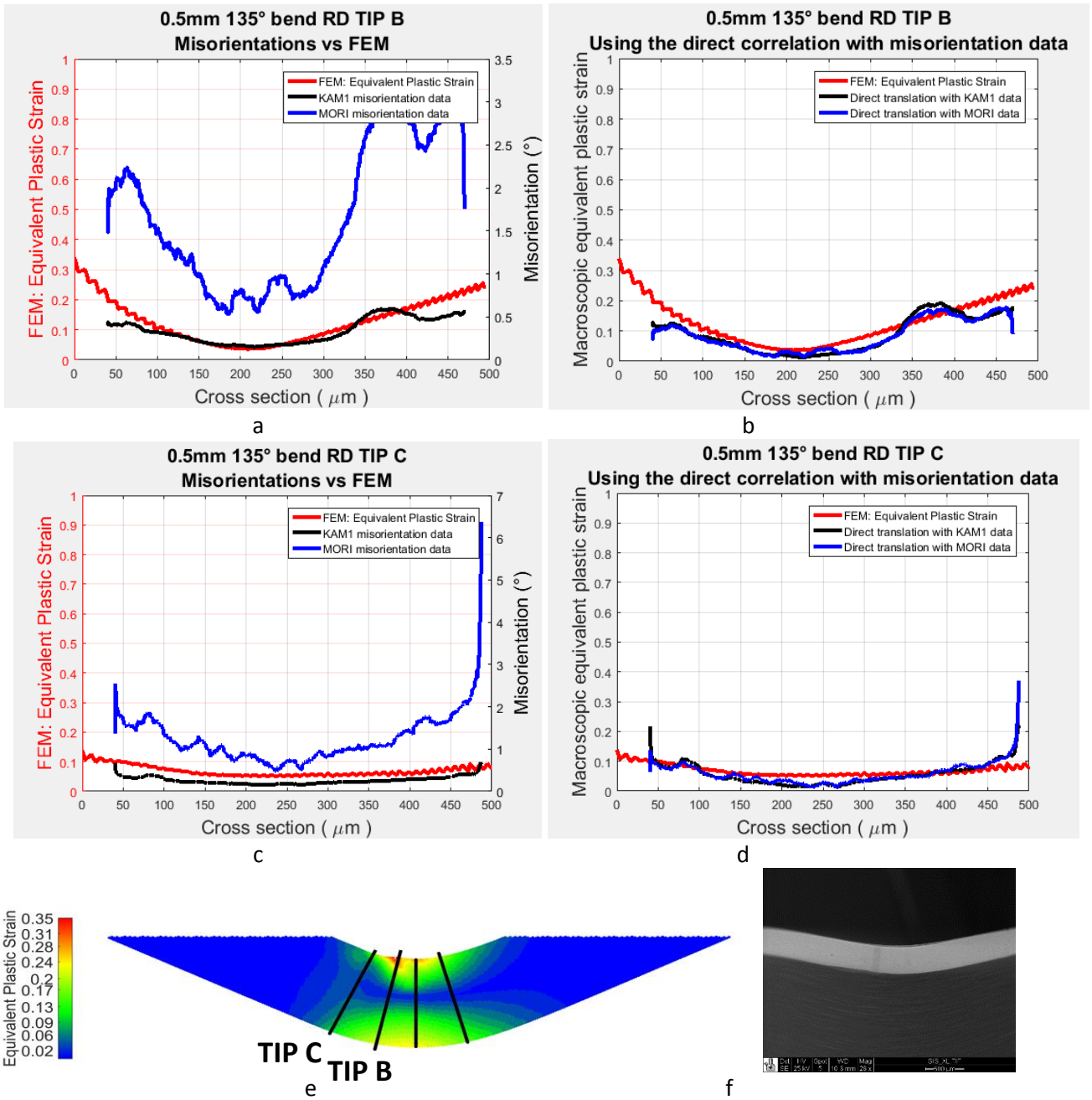

Figure 37 The results of TIP B and TIP C of the 135° 0.5 mm thick bent sample. The red line is the FEM data. a) TIP B: The misorientation data and the FEM data plotted with separate y axes. b) TIP B: ε_p derived with the misorientation and macroscopic plastic strain correlation plotted together with the FEM data. c) TIP C: The misorientation data and the FEM data plotted with separate y axes. d) TIP C: ε_p derived with the misorientation and macroscopic plastic strain correlation plotted together with the FEM data. e) The FEM results of ε_p. f) The SEM image of the sample.

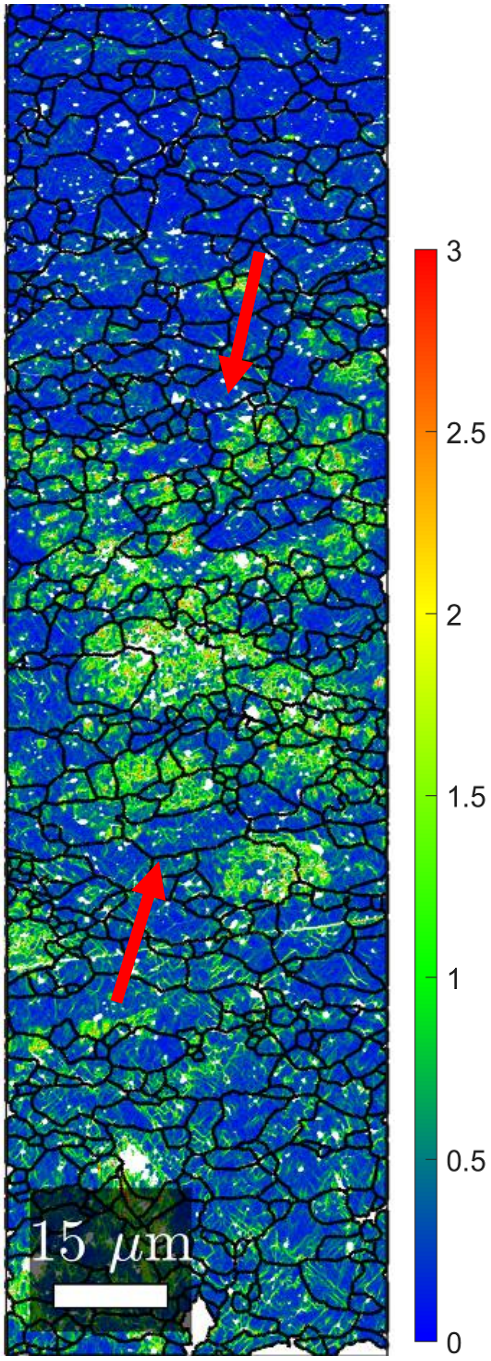

Figure 38 The KAM 1 map of the last 200 μm of the TIP B 135° bend sample scan. A large misorientation concentration forms an outlier in the Orowan fit. The bottom side of the image is the edge.

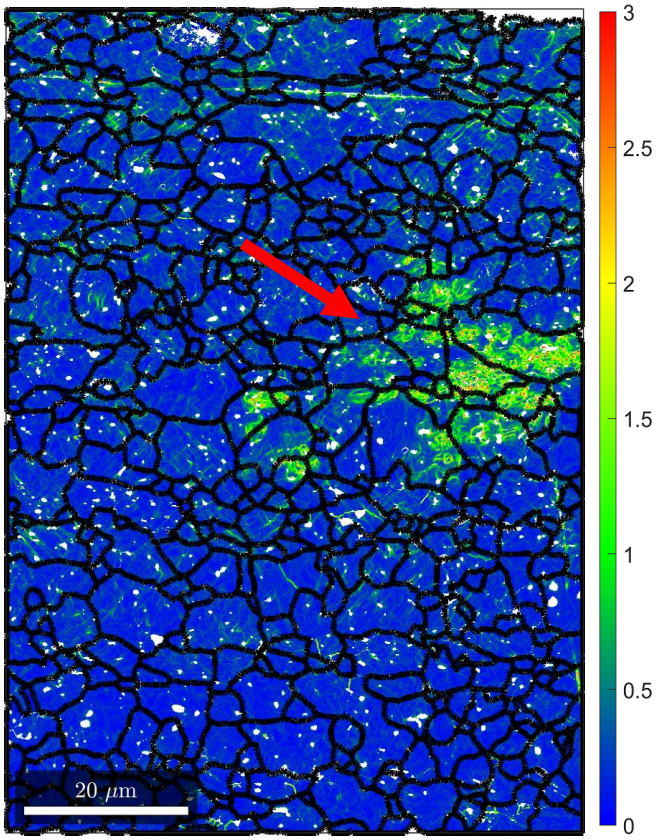

Figure 39 The KAM 1 map of the first 100 μm of the TIP C 135° bend sample scan. A large misorientation concentration forms an outlier in the Orowan fit. The top side of the image is the edge.

Finally a 60 ° bent 0.2 mm thick sample was scanned and processed. The results are shown in Figure 40. As with all the samples the edges were rounded due to the polishing which is why about 20 µm of data on each side could not be scanned. Both uses of the correlations give results that agree well with the FEM results including the low values at the center of the sample.

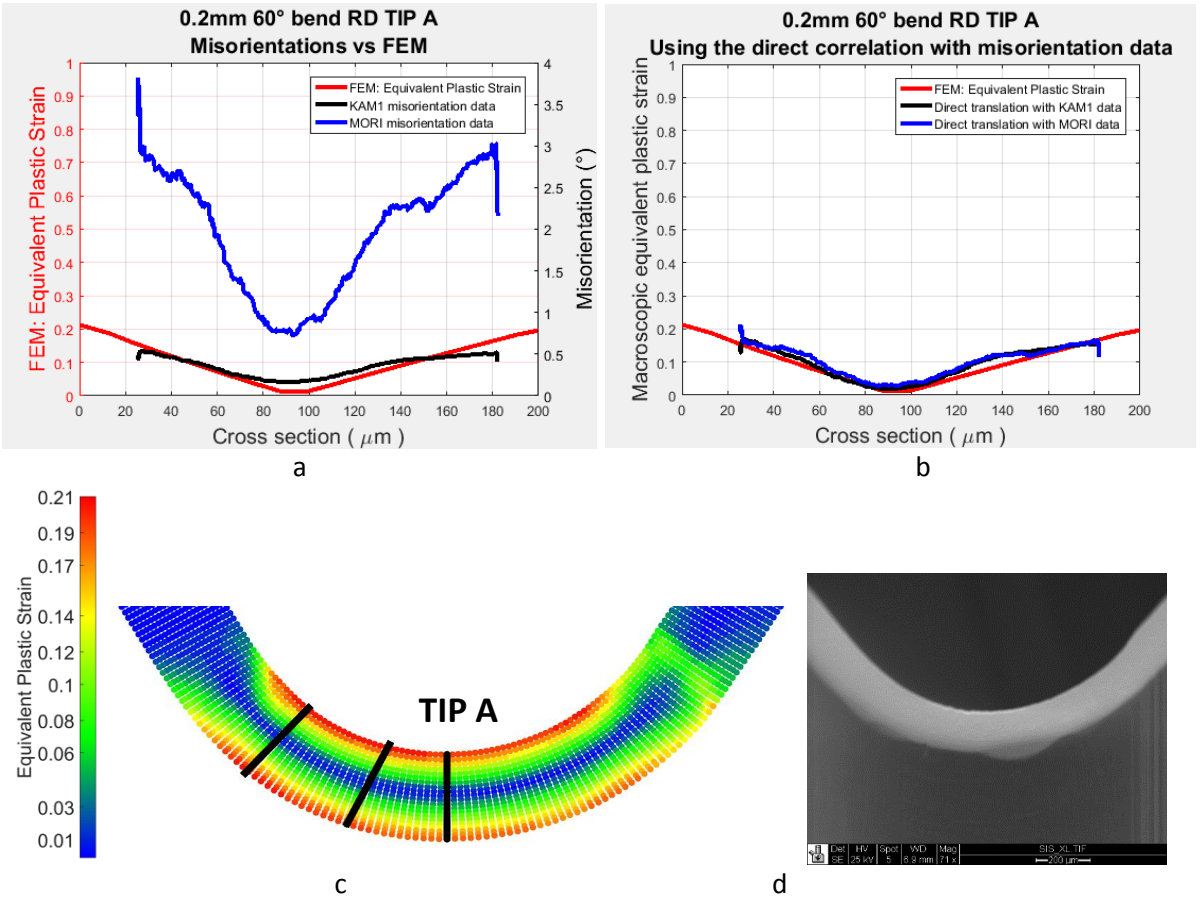

Figure 40 The results of TIP A of the 60° 0.2 mm thick bent sample. The red line is the FEM data. a) TIP A: The misorientation data and the FEM data plotted with separate y axes. b) TIP A: ε_p derived with the misorientation and macroscopic plastic strain correlation plotted together with the FEM data. c) The FEM results of ε_p. d) The SEM image of the sample.

4.3.2 The Hot Mounted Samples

The procedure of hot mounting a sample is less time consuming compared to that of cold mounting. The risk is that the high pressure present during ample mounting can contribute to the strain in the sample. To investigate this effect several scans were done on 0.5 mm and 0.2 mm thick samples.

Figure 41 shows the results of TIP A and TIP C of the 60° bended sample that was hot mounted. TIP A shows a very good agreement with the FEM data. The left side of TIP C deviates slightly, but still shows the same slope as seen in the FEM data.

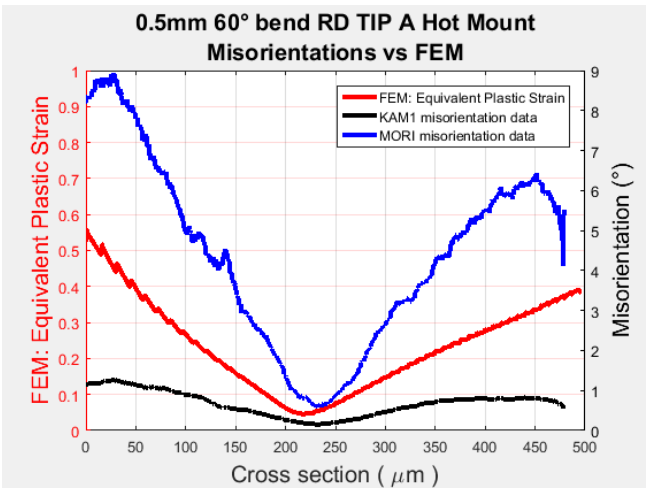

a

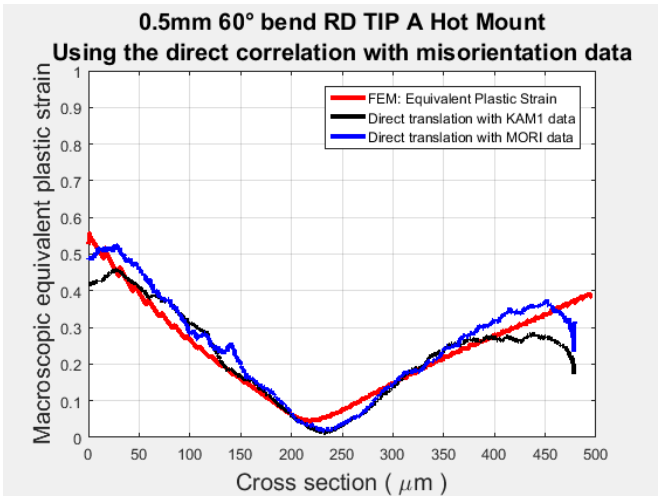

b

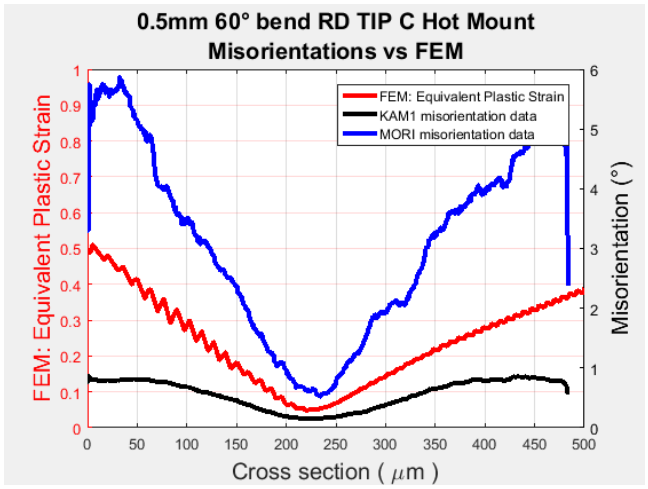

c

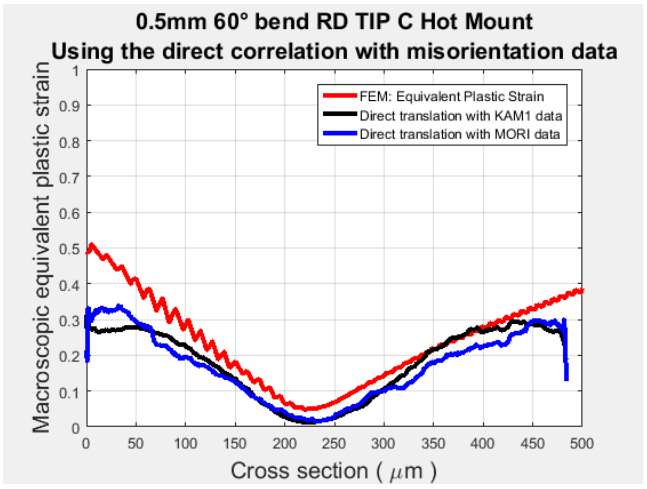

d

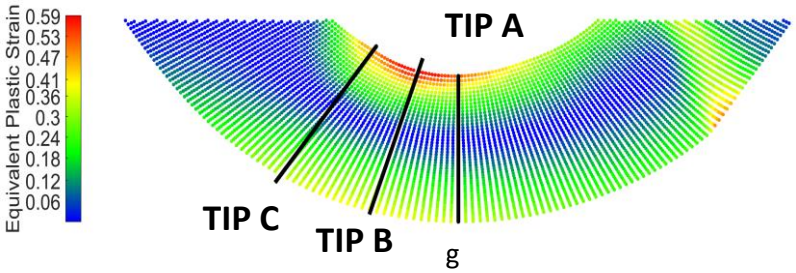

g

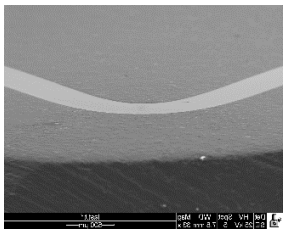

h

Figure 41 The results of TIP A and C of the 60° 0.5 mm thick hot mounted bent sample. The red line is the FEM data. a) TIP A: The misorientation data and the FEM data plotted with separate y axes. b) TIP A: ε_p derived with the misorientation and macroscopic plastic strain correlation plotted together with the FEM data. c) TIP C: The misorientation data and the FEM data plotted with separate y axes. d) TIP C: ε_p derived with the misorientation and macroscopic plastic strain correlation plotted together with the FEM data. e) The FEM results of ε_p. f) The SEM image of the sample.

Figure 42 shows the results of TIP A and TIP C of the 60° 0.2 mm bended sample that was hot mounted. The results of TIP A do not agree with FEM data very well. The slopes agree fairly well but the center sample has a strain about 5 % higher.

Overall the hot mounted data does not perform much better or worse than the cold mounted data. The possible influence of the applied pressure on the strains is not revealed in these results.

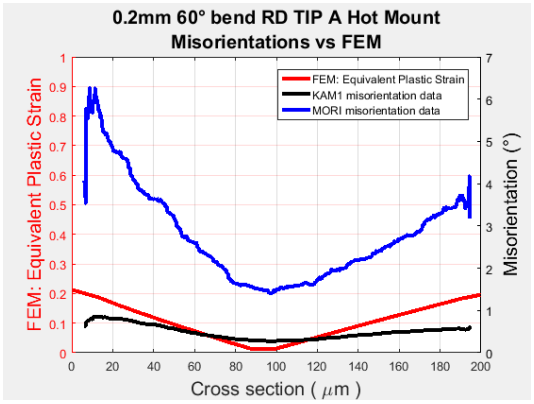

a

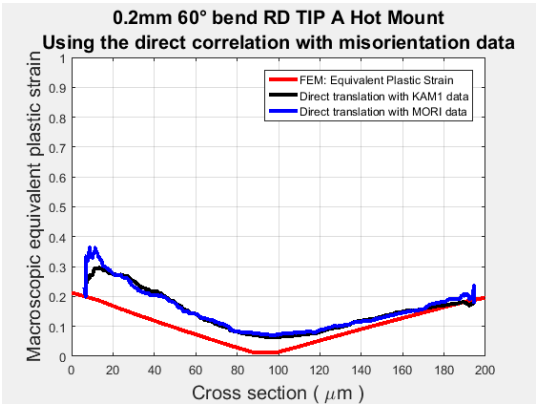

b

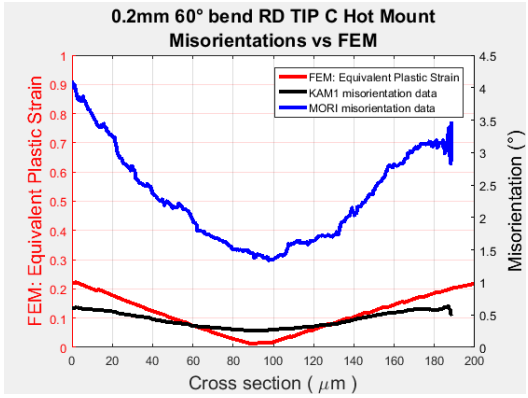

c

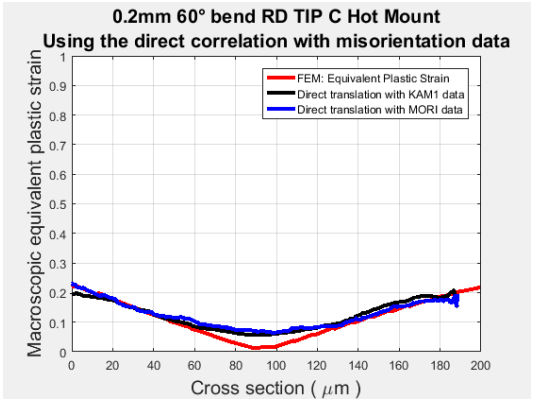

d

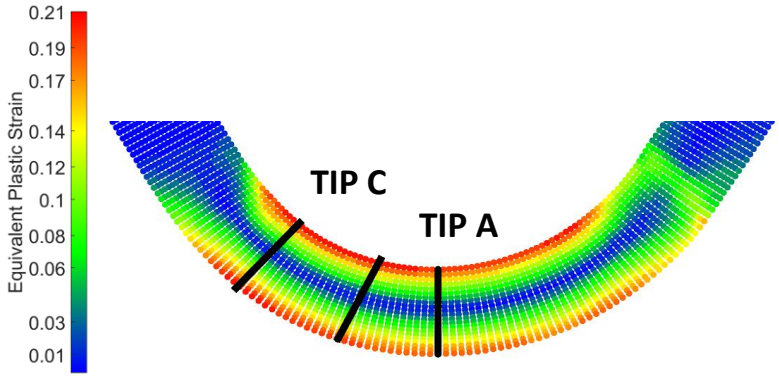

e

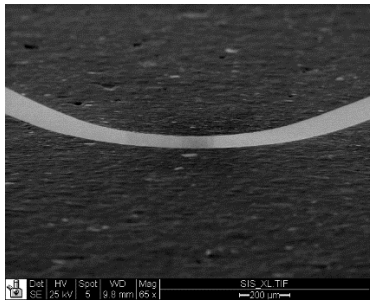

f

Figure 42 The results of TIP A and C of the 60° 0.2 mm thick hot mounted bent sample. The red line is the FEM data. a) TIP A: The misorientation data and the FEM data plotted with separate y axes. b) TIP A: ε_p derived with the misorientation and macroscopic plastic strain correlation plotted together with the FEM data. c) TIP C: The misorientation data and the FEM data plotted with separate y axes. d) TIP C: ε_p derived with the misorientation and macroscopic plastic strain correlation plotted together with the FEM data. e) The FEM results of ε_p. f) The SEM image of the sample.

4.4 The Gage R&R Results

For the gage repeat and reproducibility study an area of 25x25 µm was scanned several times according to the strategy discussed in Chapter 2.5. A location on a highly deformed sample was chosen to test the extreme case. Figure 43 shows the area that was used for reference scans. Six complete grains common in each scan were selected for the reproducibility analysis. Of the data of each grain the grain size and the average KAM 1 data was computed. Furthermore the KAM 1 data was also used to calculate the macroscopic strain using the correlation presented in section 4.2. These three data sets were used for the ANOVA.

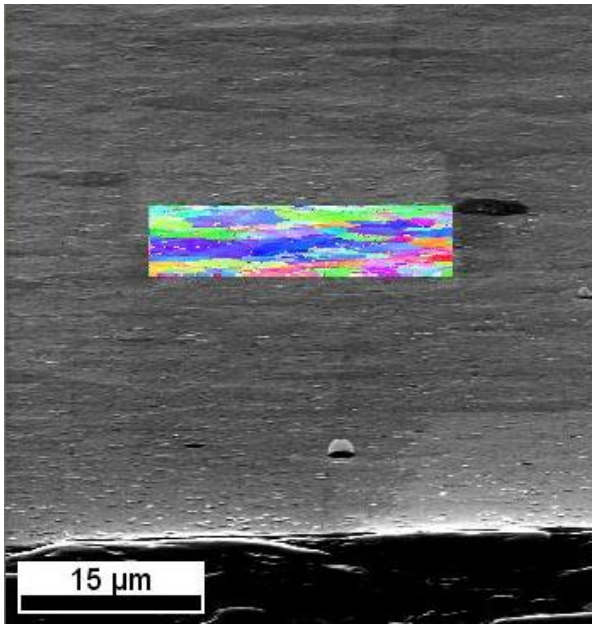

Figure 43 The scanned area for the gage R&R study. Sample: 0.5 mm 60 ° bent hot mounted sample (The sample is tilted 73 º around horizontal axis).

Figure 44 shows the relative standard deviations of the repeat (blue points), the reload factor (red points) and the total of the two (black points). They are presented in percentage of the mean value of the used data for that standard deviation. For example the percentage of error in grain size of grain 1 is calculated with respect to the mean grain size of grain 1 of all scans.

The grain size results show total errors varying from 10 to 35 % which is considerably large. This is caused by the repeat error which makes the contribution of the reload error almost negligible. The grain size is actually the number of pixels in the detected grain. Slight changes in the grain boundary of a small grain can cause large differences in the number of pixels and thus can cause a large error.

The KAM 1 data results show very small errors that are predominantly caused by reloading the sample. Even so, the total error does not exceed 0.8 %. The calculation of the macroscopic plastic strain using the KAM 1 correlation with the tensile tests shows similar results with the total error not exceeding 0.6 %. Overall the total errors of the misorientation results do not exceed 1.0 % which makes the EBSD scan equipment very reliable. The numerical results are summarized in appendix A.

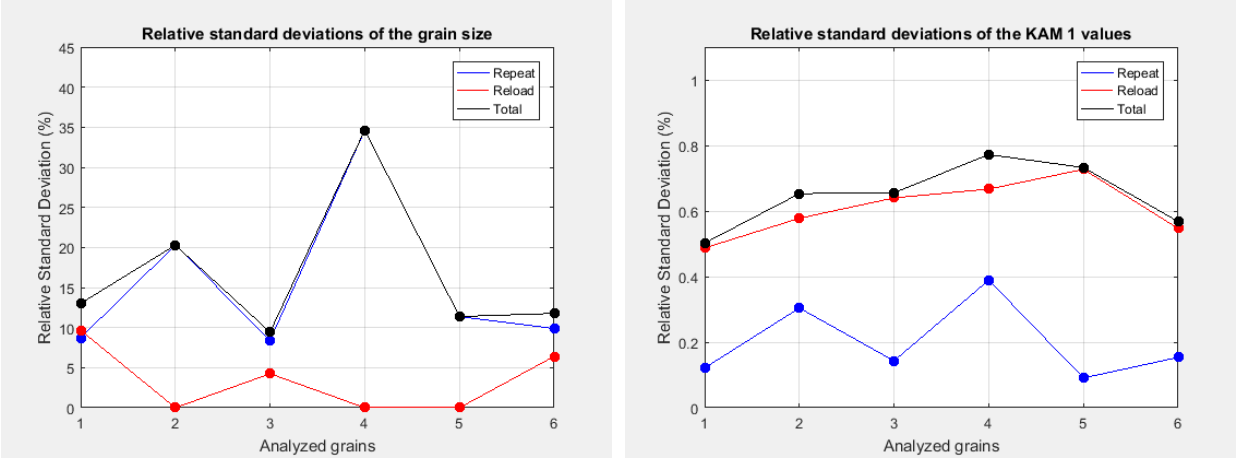

Figure 44 The standard deviations obtained with the gage R&R study of six grains. The data is shown in percentage of the mean value. Presented are the repeat error (blue), the reload error (red) and the total error (black). a) The results of the detected grain size. b) The results of the KAM 1 misorientation measurements. c) The macroscopic plastic strains calculated using the correlation of the KAM 1 data with the tensile tests.

5 Conclusions

Macroscopic plastic deformations in bent ferritic samples were successfully estimated using EBSD misorientation data. This was achieved with a correlation of misorientations and macroscopic plastic strains. These correlations were found using tensile test samples obtained with defined macroscopic plastic strains. The misorientations were processed to obtain KAM kernel 1 values and to obtain the mean misorientation with respect to the average orientation of each grain. Both misorientation data types performed well for the translation in macroscopic plastic strain. The correlations were used to calculate the macroscopic plastic strain in more complex deformed 0.2 mm and 0.5 mm thick bent samples with 40 °, 60 °, 90 ° and 135 ° angles. The results agreed quite well with finite element calculations. This proved that the relation of the misorientations with the tensile test macroscopic plastic strains in which the strains reached a maximum of 20 %, can be used to calculate macroscopic plastic strains up to 50 % obtained in more complex deformed samples.

An attempt was made to use the misorientation data to estimate the dislocation density. For this the misorientations were assumed all to be caused by glide dislocations. The dislocation density estimates were used in Orowan's equation together with a rough estimate for the dislocation traveling distance based on the grain size. The Schmid factor was used to weight the result for each grain based on the orientation of the grain. The microscopic plastic strain values resulting from this exercise were a factor 100 too high. The approach used in this exercise estimates too many dislocations for each pixel. Next to that, the real dislocation travel distance is also very difficult to estimate. The main problem with this exercise is that the misorientations are caused by many different complex interactions of different types of dislocations. The use of this dislocation density model and travel distance model for the Orowan equation to calculate the microscopic plastic strain is therefore rejected.

No clear differences in results were obtained when hot mounting was used instead of cold mounting. Elevated plastic strain levels due to the high pressures during hot mounting were not observed.

The Gage R&R study

A gage R&R study was performed with six heavily deformed grains of one of the ferritic samples. One factor was used which is the reloading of the sample in the SEM. This factor included searching the position and tuning the electron beam. From these grains three data sets were calculated and used in ANOVA studies. These were grains sizes, the KAM 1 misorientation values and the macroscopic plastic strains obtained using the direct KAM 1 and tensile test correlation. The grain size detection had the largest total error which reached up to 35 % of the mean grain size. The reload factor had no significant contribution to the total error. Slight differences in the grain boundaries of the repeated scans could have caused a large difference in the number of pixels belonging to the grain resulting in a significant grain size error. This is especially the case for small grains.

For the KAM 1 data and the directly translated macroscopic plastic strain data the reload factor did contribute significantly. However both the KAM 1 data and the macroscopic plastic strain translation had total errors that did not exceed 0.8 %. This makes the used equipment very reliable for this study.

6 Recommendations

The Tensile Tests

The tensile tests were performed with limited scan time. Considering the clear correlation of misorientations with plastic strain it is expected that the spread on the data points will decrease when more data is measured. Outlier grains that are exceptionally large or which have an exceptionally high misorientation density will be averaged out.

Some measurements were done with a second set of tensile test samples to test the repeatability of the correlation. Due to the limited scan time this could not be finished and should be completed. However the scans that were done gave almost exactly the same values as the set used in this study which suggests that the data is reliable.

More data points are needed close to the plastic strain level right before material failure to study how the correlation starts to deviate due to necking mechanisms.

Differences in EBSD scan settings are expected to have an influence on the values. This should be investigated as well. A larger gage R&R study could be performed in which these setting are used as the factors to study the influences.

The Bended Sample Tests

As with the tensile tests more data is needed. Copies of the bended samples should be tested to test the reproducibility and to average out the outliers that caused spikes in the plastic strain signal.

The quality of the EBSD indexing could be further improved by making scans with a zoom larger than 2000x instead of the 1000x currently used. However the patching of multiple scans is challenging and a reference point technique should be implemented to know the exact scan locations. Also the spot size (~2 nA) should be reduced.

Finally samples with larger thicknesses should be studied which will have even higher plastic strains on the edges to study up to what strain values the tensile test correlation successfully translates the misorientations in macroscopic plastic train. Caution is needed not to bend the samples with an angle that will cause cracks at the tips.

Acknowledgements

This report is a master thesis and was written as a conclusion of the masters in material science. I would like to thank Professor Doctor Jeff Th. M. De Hosson for the opportunity of do this research in his metallurgy research group at the Rijksuniversiteit Groningen in the Netherlands where I have been welcomed by a very friendly and open group.

Special thanks to Doctor Václav Ocelík for his courses in scanning electron microscopy and electron backscatter diffraction. He always had time to explain and give tips on the best way to prepare samples and how to improve scan qualities.

Furthermore I would like to thank Doctor Indranil Basu for many indebt metallurgic discussions and advise on how to model dislocation densities. I would also like to thank Herman Fidder MSc. for his training in preparing and polishing of the samples.

Of the people outside the Rijksuniversiteit Groningen I would like to thank Paul Huizenga MSc. for the opportunity to do this research with the support of Philips and Mark Veldhuis MSc. for the training in Marc Mentat (MSC) and many hours of lessons in mechanical theory and metallurgy.

Thank you all very much!

References

[1] Kamaya, M. (2009). Measurement of local plastic strain distribution of stainless steel by electron backscatter diffraction. *Materials Characterization*, *60*(2), 125-132.

[2] Gao, H., Huang, Y., Nix, W. D., & Hutchinson, J. W. (1999). Mechanism-based strain gradient plasticity—I. Theory. *Journal of the Mechanics and Physics of Solids*, *47*(6), 1239-1263.

[3] Kubin, L. P., & Mortensen, A. (2003). Geometrically necessary dislocations and strain-gradient plasticity: a few critical issues. *Scripta materialia*, *48*(2), 119-125.

[4] Konijnenberg, P. J., Zaefferer, S., & Raabe, D. (2015). Assessment of geometrically necessary dislocation levels derived by 3D EBSD. *Acta Materialia*, *99*, 402-414.

[5] Kamaya, M. (2011). Assessment of local deformation using EBSD: Quantification of accuracy of measurement and definition of local gradient. *Ultramicroscopy*, *111*(8), 1189-1199.

[6] Kamaya, M., Wilkinson, A. J., & Titchmarsh, J. M. (2005). Measurement of plastic strain of polycrystalline material by electron backscatter diffraction. *Nuclear engineering and design*, *235*(6), 713-725.

[7] Kamaya, M., Wilkinson, A. J., & Titchmarsh, J. M. (2006). Quantification of plastic strain of stainless steel and nickel alloy by electron backscatter diffraction. *Acta Materialia*, *54*(2), 539-548.

[8] Brewer, L. N., Field, D. P., & Merriman, C. C. (2009). Mapping and assessing plastic deformation using EBSD. In *Electron backscatter diffraction in materials science* (pp. 251-262). Springer, Boston, MA.

[9] Hull, D., & Bacon, D. J. (2001). *Introduction to dislocations*. Butterworth-Heinemann.

[10] Randle, V. (1992). Microtexture determination and its applications. *Maney for the Institute of Materials, Minerals and Mining*, 2003

[11] Zijlstra, G. (2014) Microscopy study of the onset of plastic deformation and modeling creep behavior of AISI 420 stainless steel, *Master Thesis*, Rijksuniversiteit Groningen

[12] Davis, J. R. (Ed.). (1994). *Stainless steels*. ASM international.

[13] Zhou, X-H., and Gao, S. (1997), "Confidence intervals for the log-normal mean," *Statistics in Medicine*, 16, 783-790.

Appendix A – The Gage R&R Results

In this appendix the numerical results of the gage repeat and reproducibility are presented for the six grains that were selected.

Relative standard deviations of the grain size measurements

	Grain 1	**Grain 2**	**Grain 3**	**Grain 4**	**Grain 5**	**Grain 6**
p value	0,0843	0,7307	0,2789	0,6820	0,6002	0,2172
reload variance (% of the mean)	93,329	0,000	18,019	0,000	0,000	41,051
reload stdev (% of the mean)	9,661	0,000	4,245	0,000	0,000	6,407
error variance (% of the mean)	76,016	411,594	71,007	1199,267	129,435	97,516
error stdev (% of the mean)	8,719	20,288	8,427	34,630	11,377	9,875
total variance (% of the mean)	2220,325	1737,287	447,802	6603,067	738,259	2241,668
total stdev (% of the mean)	13,013	17,527	9,435	30,518	10,395	11,771

Relative standard deviations of the KAM 1 measurements

	Grain 1	**Grain 2**	**Grain 3**	**Grain 4**	**Grain 5**	**Grain 6**
p value	0,0007	0,0163	0,0004	0,0235	0,0000	0,0012
reload variance (% of the mean)	0,237	0,334	0,410	0,445	0,529	0,299
reload stdev (% of the mean)	0,487	0,578	0,640	0,667	0,727	0,547
error variance (% of the mean)	0,015	0,092	0,020	0,151	0,008	0,024
error stdev (% of the mean)	0,121	0,304	0,143	0,389	0,091	0,154
total variance (% of the mean)	0,001	0,003	0,002	0,005	0,004	0,003
total stdev (% of the mean)	0,502	0,653	0,656	0,772	0,733	0,568

Relative standard deviations of the macroscopic plastic strain when using the correlation with KAM1

	Grain 1	**Grain 2**	**Grain 3**	**Grain 4**	**Grain 5**	**Grain 6**
p value	0,0007	0,0163	0,0004	0,0235	0,0000	0,0012
reload variance (% of the mean)	0,130	0,172	0,231	0,223	0,276	0,148
reload stdev (% of the mean)	0,361	0,415	0,481	0,472	0,525	0,385
error variance (% of the mean)	0,008	0,048	0,012	0,076	0,004	0,012
error stdev (% of the mean)	0,090	0,218	0,107	0,275	0,065	0,108
total variance (% of the mean)	0,000	0,001	0,000	0,001	0,001	0,001
total stdev (% of the mean)	0,372	0,469	0,493	0,546	0,529	0,400